Acta Pharmaceutica Sinica B 2023;13(12):4875–4892

Chinese Pharmaceutical Association
Institute of Materia Medica, Chinese Academy of Medical Sciences

Acta Pharmaceutica Sinica B

www.elsevier.com/locate/apsb
www.sciencedirect.com

ORIGINAL ARTICLE

Sorting nexin 3 exacerbates doxorubicin-induced cardiomyopathy *via* regulation of TFRC-dependent ferroptosis

Wenjing Yu[a,b,†], Yuehuai Hu[a,b,†], Zhiping Liu[c,†], Kaiteng Guo[a], Dinghu Ma[a], Mingxia Peng[a], Yuemei Wang[a], Jing Zhang[a], Xiaolei Zhang[a], Panxia Wang[a], Jiguo Zhang[d], Peiqing Liu[a,b,d,*], Jing Lu[a,b,*]

[a]*National and Local United Engineering Lab of Druggability and New Drugs Evaluation, School of Pharmaceutical Sciences, Sun Yat-sen University, Guangzhou 510006, China*
[b]*Guangdong Provincial Key Laboratory of New Drug Design and Evaluation, Guangdong Province Engineering Laboratory for Druggability and New Drug Evaluation, School of Pharmaceutical Sciences, Sun Yat-sen University, Guangzhou 510006, China*
[c]*School of Pharmacy, Jinan University, Guangzhou 510632, China*
[d]*School of Pharmaceutical Sciences, Shandong First Medical University & Shangdong Academy of Medical Sciences, Taian 271016, China*

Received 17 January 2023; received in revised form 6 June 2023; accepted 13 June 2023

KEY WORDS

SNX3;
Ferroptosis;
TFRC;
Cardiomyopathy;
Doxorubicin;
Iron homeostasis;
Cell death;
Mitochondria

Abstract The clinical utilization of doxorubicin (Dox) in various malignancies is restrained by its major adverse effect: irreversible cardiomyopathy. Extensive studies have been done to explore the prevention of Dox cardiomyopathy. Currently, ferroptosis has been shown to participate in the incidence and development of Dox cardiomyopathy. Sorting Nexin 3 (SNX3), the retromer-associated cargo binding protein with important physiological functions, was identified as a potent therapeutic target for cardiac hypertrophy in our previous study. However, few study has shown whether SNX3 plays a critical role in Dox-induced cardiomyopathy. In this study, a decreased level of SNX3 in Dox-induced cardiomyopathy was observed. Cardiac-specific *Snx3* knockout (*Snx3*-cKO) significantly alleviated cardiomyopathy by downregulating Dox-induced ferroptosis significantly. SNX3 was further demonstrated to exacerbate Dox-induced cardiomyopathy *via* induction of ferroptosis *in vivo* and *in vitro*, and cardiac-specific *Snx3*

*Corresponding authors.
E-mail addresses: liupq@mail.sysu.edu.cn (Peiqing Liu), lujing28@mail.sysu.edu.cn (Jing Lu).
[†]These authors made equal contributions to this paper.
Peer review under the responsibility of Chinese Pharmaceutical Association and Institute of Materia Medica, Chinese Academy of Medical Sciences.

https://doi.org/10.1016/j.apsb.2023.08.016

transgenic (*Snx3*-cTg) mice were more susceptible to Dox-induced ferroptosis and cardiomyopathy. Mechanistically, SNX3 facilitated the recycling of transferrin 1 receptor (TFRC) *via* direct interaction, disrupting iron homeostasis, increasing the accumulation of iron, triggering ferroptosis, and eventually exacerbating Dox-induced cardiomyopathy. Overall, these findings established a direct SNX3−TFRC −ferroptosis positive regulatory axis in Dox-induced cardiomyopathy and suggested that targeting SNX3 provided a new effective therapeutic strategy for Dox-induced cardiomyopathy through TFRC-dependent ferroptosis.

1. Introduction

Doxorubicin (Dox), one of the most prescribed anthracycline chemicals, is widely employed to treat various solid tumors and hematological malignancies[1,2]. Nevertheless, the clinical application of Dox is restricted by its dose-dependent irreversible cardiotoxic effects, which are accompanied by myocardial cell death[2−4]. The etiopathogenesis of Dox-induced cardiomyopathy is disputable and complicated but may have three main characteristics: redox cycling, mitochondrial toxicity, and myocyte death[5−7]. Oxidative stress is thought to be a major contributor to Dox-induced cardiomyopathy; however, antioxidant therapy using reactive oxygen species (ROS) scavengers only offers modest protection[6,8]. Mitochondrial toxicity is also considered a key factor in Dox-induced cardiomyopathy[6]. Both ROS production and mitochondrial toxicity result in cardiomyocyte death[6−8]. Cardiomyocytes are terminally differentiated cells that exhibit different modes of death, including apoptosis (which we have previously reported[9]), autophagy, necrosis, as well as ferroptosis which is newly characterized[10,11], and not fully illuminated. Indeed, the mitochondria-targeted antioxidant MitoTEMPO substantially rescues Dox-induced cardiomyopathy, since sustaining mitochondrial oxidative damage is considered a major mechanism in ferroptosis-induced heart injury[12]. Accumulating evidence suggests that Dox-induced cardiomyocyte ferroptosis results from aberrant iron accumulation in cardiac mitochondria[7,13]. Since ferroptosis differs from other types of programmed cell death (PCD) which depending on their own routine cellular signaling pathways, suppression of ferroptosis might provide an alternative strategy that bypasses the apoptosis or necrosis pathway to improve the survival of Dox-induced cardiomyocyte death[14,15].

Ferroptosis, is involved in various diseases due to its important physiological and pathological effects, such as cancer, stroke, Dox-induced cardiomyopathy and chronic ischemia/reperfusion injury[7,16−18]. Ferroptosis is a new identified type of PCD associated with excessive lipid peroxides and excessive iron-dependent accumulation, involving iron metabolism, amino acid metabolism, and lipid metabolism[12,19,20]. The iron homeostasis and lipid peroxide imbalance arising from excess ROS accumulation are hallmarks of ferroptosis[12]. Recent studies have revealed that the induction of ferroptosis depends on intracellular iron level and metabolism[21]. Specifically, iron metabolism includes four aspects: import, export, storage, and turnover[21,22]. During the processes of cellular iron transport and metabolism, ferric iron (Fe^{3+}) binds to transferrin in a soluble state and enters the intracellular region. With the assistance of TFRC, Fe^{3+} crosses the endosomal membrane and subsequently reduces to divalent iron (Fe^{2+}); finally, Fe^{2+} is able to enter the cytoplasmic labile iron pool[23,24]. Supernumerary Fe^{2+} in labile iron pool can produce ROS *via* Fenton and induce ferroptosis; in addition, intracellular iron can be absorbed and utilized by binding to cytoplasmic divalent metal transporter 1 and TFRC. Disruption in iron homeostasis affects various cardiovascular diseases[21]. For example, iron-dependent ferroptosis aggravates cardiac injury[25,26]. Hence, targeting the iron transporters, like TFRC, may be key targets for Dox-induced cardiomyopathy through modulating ferroptosis sensitivity.

The sorting nexins family is characterized by the Phox homology (PX) domain and coordinates retrograde transportation of cargo proteins between endosome and the trans-Golgi network (TGN) or plasma membrane (PM)[27]. In general, sorting nexins and vacuolar protein sorting (VPS) bind to cargo proteins and form retromer complexes that are located in the endosomal membrane *via* the PX domain[27]. For instance, the SNX1−retromer complex cooperates with Rab7-GTP to mediate the Rab-GAP protein (TBC1D5) degradation pathway[28,29]. SNX3 and VPS26−VPS29−VPS35 form a "T" type SNX3−retromer complex to mediate recycling of Wntless protein to the TGN[30,31]. The PX domain structure of SNX3 is liable for membrane trafficking, cell signaling, which profoundly affects cardiac performance[32,33]. Our laboratory recently reported that SNX3-retromer regulated nuclear translocation of the signal transducer and activator of transcription 3 (STAT3) and played a critical role in pathological cardiac hypertrophy[34]. However, the specific roles and mechanisms of SNX3 in determining the destination of cargo proteins in Dox-induced cardiomyopathy have not been elucidated.

2. Methods

2.1. Animals

All animal experiments performed in this study were approved by Research Ethics Committee of Sun Yat-sen University and conformed to Guide for the Care and Use of Laboratory Animals (NIH Publication No. 85−23, revised 1996). Wild-type C57BL/6 mice (8−10 weeks) were purchased from the Laboratory Animal Center of Sun Yat-sen University. *Snx3*-cKO mice and *Snx3*-cTg mice were generated by using the CRISPR/Cas9 technology at the Shanghai Model Organisms Center, as described earlier[34], $Snx3^{flox/flox}$ mice were crossed with C57BL/6J-$Myh6^{em1(IRES\text{-}Cre)Smoc}$ mice to generate $Snx3^{flox/flox}$ *Myh6-Cre*$^{+}$ mice (*Snx3*-cKO mice). The Piggybac vector harboring mouse SNX3 cDNA was microinjected into the fertilized egg of C57BL/6 mice to obtain

the transgenic founder mice and then crossed with B6.FVBTg (*Myh6-Cre*) 2182 Md/J mice to generate *Snx3*-cTg mice.

All the generated mice were housed in temperature-controlled cages under a 12-h light−dark cycle and given free access to water and normal chow diet. At the endpoint of experiment, all mice were euthanized by injecting sodium pentobarbital (150 mg/kg, Merck) intraperitoneally. The experimental procedures were implemented in accordance with the China Animal Welfare Legislation, reviewed and approved by the Sun Yat-sen University Committee on Ethics in the Care and Use of Laboratory.

2.2. *In vivo drug administration and AAV9 transduction*

Only male mice were utilized in our research because of a marked sex difference in Dox-induced cardiotoxicity[3]. All mice were randomly assigned to each group. For Dox treatment, as described before[35], 3 months-old male mice were weighted and injected intraperitoneal (i.p.) at an accumulative dose of 24 mg/kg for 2 weeks. For Deferoxamine (DFO) treatment, DFO was dissolved in 15% castor oil and further diluted in PBS, and DFO (100 mg/kg) or corresponding vehicle (15% castor oil) was administered intraperitoneally to 3-month-old male mice thrice a week for 4 weeks. Mice in the Dox + DFO group were given thrice a week i.p. injection of DFO (100 mg/kg) or vehicle 3 weeks before Dox treatment, and then 3 weeks after treatment with DFO, the mice were randomly allotted to inject Dox or saline for the last week.

Adeno-associated virus 9 (AAV9) vectors shRNA-*Gfp* (sh-NC) or shRNA-*Tfrc* (sh-TFRC) for gene knockdown were purchased from Vigene. Male mice were intramyocardially injected at three to five sites with AAV9 sh-NC or sh-TFRC at a dose of 20 μL of virus containing 10^{11} viral genome particlesper mouse using an insulin syringe with a 30-gauge needle.

2.3. *Cardiac functions examination*

At the end of the treatment, the mice heart function was examined through echocardiography by Vevo 2100 Imaging System (VisualSonics). Cardiac ventricular structure and systolic function were examined by two-dimensional imaging motion mode to record parasternal short-axis fields. Parameters included the left ventricular (LV) anterior wall thickness in the end-diastolic/end-systolic stages, the LV posterior wall thickness, the LV internal diameter; LV ejection fraction, and LV fractional shortening, cardiac output, stroke volume. Tissue Doppler imaging was applied to observe the rate of the mitral annular motion to evaluate cardiac diastolic function. Four waves mainly assess diastolic function: isovolumic relaxation time, isovolumic contraction time, mitral valve (MV) motion in early left ventricular diastole (E'), and atrial contraction during late left ventricular (A').

2.4. *Histology and immunohistochemistry (IHC) analyses*

The myocardial tissue of the mice was excised, and the upper part was fixed in 4% paraformaldehyde overnight and then embedded in paraffin for morphometric measurement. Hematoxylin−eosin (HE) staining for morphological analyses, Masson's trichrome staining or picric sirius red (PSR) staining for collagen sediment assessments according to standard histological protocols, and prussian blue (Perl) stain to show free Fe^{2+} in heart tissue. Photomicrographs were captured using EVOS FL Auto Cell Imaging System (Thermo Fisher Scientific).

IHC were performed for SNX3 and 4-hydroxynonena (4-HNE) staining. Heart tissues were fixed in 4% phenol-formaldehyde adhesive, embedded in paraffin and sectioned at 5-μm thickness. The following primary and secondary antibodies were used: anti-SNX3 (K009182P; Solarbio), anti-4-HNE (ab46545; Abcam), secondary antibody (7074S, 7076S; CST).

2.5. *Immunofluorescence (IF) staining*

Fixing and blocking methods were consistent with IHC analysis and then incubated at 4 °C with anti-SNX3 (10772-1-AP; Proteintech) and anti-cTnT (ab8295; Abcam) overnight. Tissue sections were incubated with fluorescent secondary antibodies (4412S, 8890S; CST) for 1 h at room temperature. Finally, DAPI (4083; CST) was used to label the nuclei. Fluorescence was detected below the FV3000 fluorescent microscope (OLYMPUS).

2.6. *DHE for ROS analysis*

Heart tissue was snap-frozen and embedded in an optimal cutting temperature compound. 5-μm thickness sections were made by a freezing microtome slicer for dihydroethidium (DHE) staining. Sections were incubated with DHE (S0063, 1:500, Beyotime) at 37 °C for 20 min in the dark, and then washed with PBS for 5 min. Subsequently, sections were incubated for 10 min at room temperature and then sealed with an anti-fluorescence quenching sealant. Images were obtained using the FV3000 fluorescent microscope.

2.7. *Neonatal rat cardiomyocytes culture and in vitro treatment*

As previously reported, neonatal rat cardiomyocytes (NRCMs) were cultured from 1 to 3 days of Sprague−Dawley rats. The hearts were immediately isolated and digested with 0.08% trypsin to prepare single cell suspension. NRCMs were maintained in Dulbecco's modified Eagle's medium (Gibco) carrying 10% fetal bovine serum (Gibco) and 1% 5-bromodeoxyuridine (Thermo Fisher Scientific) and cultured in 5% CO_2 standard incubator at 37 °C.

The NRCMs were treated after 48 h of static culture, Dox (1 μmol/L), DFO (100 μmol/L), ferrostatin-1 (Fer-1, 3 μmol/L) and Erastin (10 μmol/L) were applied at indicated concentrations.

Methods of transfecting NRCMs with adenovirus or plasmid or small interfering RNAs were as previously reported. Recombinant adenoviral vectors expressing rat SNX3 (Ad-SNX3, with Flag-tag), rat sh-SNX3 sequence (Ad-sh-SNX3, with Flag-tag) and control vectors were generated by standard procedures. Ad-SNX3, Ad-shSNX3, and Ad-vector were purchased from Vigene. *Snx3* (NM_001044283.1) and *Tfrc* (NM_022712.1) were built by ligating respective full-length cDNA into pcDNA3.1$^{(+)}$ with Flag-tag or HA-tag. Small interfering RNAs targeting SNX3 (si-*Snx3*) and TFRC (si-*Tfrc*) were bought from GenePharma. Then, the possibility of overexpression or deletion was measured by quantitative RT-PCR or Western blotting.

2.8. *Western blotting and pull-down assays*

Myocardial tissues or NRCMs were covered with RIPA lysis buffer (Beyotime) for 10 min. Equal protein samples were loaded, separated by sodium dodecyl sulfate-polyacrylamide gel electrophoresis, and transmitted to polyvinylidene fluoride membranes (Millipore). The membranes were blocked in skim milk and

incubated with primary antibodies and then with secondary antibodies. Signs at the protein level were observed using an enhanced chemiluminescence system (Tanon) and quantitatively examined by ImageJ software. The relevant antibodies used were as follows: SNX3 (10772-1-AP; Proteintech), SNX3 (sc-376,667; Santa Cruz), TFRC (ab269513; Abcam), 4-HNE (ab46545; Abcam), His-Tag (2365; CST), HA-Tag (3724; CST), Anti-Flag (F1804; Sigma), α-tubulin (66031-1-Ig; Proteintech), and anti-mouse or anti-rabbit IgG HRP-linked secondary antibodies (7076, 7074; CST).

For His pull-down assay, fusion His-SNX3 proteins expressed by *E. coli* BL21 were respectively purged by His-Tag Immunomagnetic Beads (GenScript). His-SNX3 proteins were induced with cell lysates of SNX3 or TFRC protein overexpressed by plasmid for 4 °C overnight and then added His-beads for incubation 2 h at room temperature. The beads were washed with washing buffer, added elution buffer for denaturation, and boiled in a metal bath for 5 min. Finally, immunoprecipitated proteins were examined by Western blotting.

2.9. Transmission electron microscopy (TEM)

Heart tissue was cut from the left ventricle into fragments of approximately 1 mm^3 and rapidly fixed in 2.5% glutaraldehyde solution (Servicebio) for 2 h at room temperature in the dark. The samples were then embedded, segmented, installed, and dyed for imaging. The mitochondrial ultrastructure was analyzed by the JEM-1400 series 120 kV Transmission Electron Microscope (JEOL).

2.10. In situ Duolink proximity ligation assay (PLA)

NRCMs were cultured overnight on confocal dishes and infected with Ad-SNX3 and plasmid of TFRC for 48 h. After treatment, the cells were fixed with 4% paraformaldehyde (Solarbio) for 10 min and permeabilized with 0.3% Triton X-100 (Beyotime) for 10 min at room temperature. Then, cells were blocked with PLA blocking buffer for 1 h at 37 °C and incubated with mouse anti-TFRC (ab269513; Abcam) and rabbit anti-SNX3 (10772-1-AP; Proteintech) overnight at 4 °C. NRCMs were added to the Duolink® In Situ Red Starter Mouse/Rabbit kit (DUO92101; Sigma) following the manufacturer's manuals. NRCMs were covered with the Anti-Mouse MINUS and Anti-Rabbit PLUS for 1 h at 37 °C, then ligation and amplification. Nuclei were stained with DAPI for 15 min at room temperature. The PLA signals were observed as distinct red fluorescent spots and were assayed by an FV3000 fluorescent microscope.

2.11. ROS production in intracellular and mitochondrial assay

To assess the relationship between mitochondrial membrane potential and mitochondrial ROS (MitoROS) production, the NRCMs were co-incubated JC-1 (MT09, Dojindo) and mtSOX Deep Red (MT14, Dojindo) in the light of the manufacturer's specifications, respectively. MitoROS was observed according to the purple fluorescence intensity (Ex: 633 nm) FV3000 fluorescent microscope.

2.12. Lipid peroxidation assay

The malondialdehyde (MDA) assay kit (Beyotime) was applied per the manufacturer's instructions to detect lipid peroxidation levels in myocardial tissues or NRCMs. Lipid peroxidation in NRCMs was indicated by C11-BODIPY581/591 (D3861; Invitrogen) staining or Liperfluo (L248; Dojindo) staining. For performing C11-BODIPY581/591, NRCMs were grown in 6-well plates overnight, then were incubated with HBSS (Gibco) containing C11-BODIPY581/591 (5 μmol/L) for 30 min at 37 °C in darkness. After harvesting by trypsinization, cells were washed, then analyzed by the FITC channel of the CytoFLEX S flow cytometer (Beckman Coulter). To LiperFluo staining, NRCMs were seeded in confocal dishes and were covered with Liperfluo (1 μmol/L) for 30 min at 37 °C darkness, and imaged by FV3000 fluorescent microscope.

2.13. Iron content detection

Iron levels in myocardial tissue were detected by the Iron Assay Kit-Colorimetric (I291, Dojindo), referring to the manufacturer's manuals. FerroOrange (F374, Dojindo) was used to detect intracellular Fe^{2+}. In detail NRCMs were cultured in confocal dishes, washed by HBSS, and then incubated with the FerroOrange (1 μmol/L) in HBSS for 30 min at 37 °C. The levels of Fe^{2+} concentrations were analyzed by the ECD channel of the CytoFLEX S flow cytometer or observed at orange fluorescence intensity (Ex: 561 nm) under the FV3000 fluorescent microscope.

2.14. Mitochondrial morphology and membrane potential

Mitochondrial morphology staining was performed according to the instructions of Mito Tracker Red (Invitrogen), Briefly, cells were stained with Mito Tracker Red (200 nmol/L) for 30 min at 37 °C.

The mitochondrial membrane potential was measured by JC-1 MitoMP Detection Kit (MT09, Dojindo) or TMRE (87917, Sigma) staining. Frozen heart slides were stained with JC-1 (5 μmol/L) for 30 min and washed with HBSS. After drying, the slides were sealed with anti-fluorescence quenching sealing tablets and analyzed with the FV3000 fluorescent microscope.

2.15. Cell viability and morphology assay

Cell counting kit-8 (CCK8) was determined for cell viability, and NRCMs were seeded on 96-well plates. After treatment, 100 μL CCK-8 solution (C0039, Beyotime) was added to each well and incubated for 4 h in a cell incubator. The optical density was measured at 450 nm by Varioskan LUX multiscan spectrum (Thermo Fisher Scientific) and was calculated as a percentage to the control group to indicate cell viability. At the same time, cell morphology was recorded under EVOS FL Auto Cell Imaging System.

2.16. Statistical analysis

The experimental data are presented as the mean ± standard error of mean (SEM). Statistical analysis was performed using GraphPad Prism 8.0 software. The two-tailed unpaired Student's *t* test was applied to compare the significant difference between the two groups. In the results with more than two groups, one- or two-way analysis of variance (ANOVA) followed by Bonferroni *post hoc* test was applied to analyze the difference when appropriate. Differences with P value < 0.05 are considered significant.

3. Results

3.1. *SNX3 was downregulated in Dox-induced cardiomyopathy*

First, mouse model of Dox-induced cardiomyopathy was successfully generated by i.p. injecting an accumulated dose of 24 mg/kg Dox three times (on Days 1, 6, and 11) for two weeks. Morphological examination revealed that the gross hearts in the Dox group were visibly smaller than those in the control group (Supporting Information Fig. S1A and S1B), and the heart weight to tibia length ratio (HW/TL) was significantly reduced in the Dox group (Fig. S1C−S1F). The echocardiography results demonstrate a downward trend of cardiac systolic and diastolic function in the Dox group (Fig. 1A and B), as evidenced by significantly decreased ejection fraction (Fig. 1C), decreased fractional shortening (Fig. 1D), decreased stroke volume (Fig. S1G), and decreased MV E'/A' ratio (Fig. S1H) after Dox treatment. HE staining (Fig. S1I) and Masson's trichrome staining (Fig. S1J) illustrated that Dox treatment also exacerbated cardiomyocyte tissue disorders and cardiac fibrosis relative to the control treatment. These results indicate that we successfully established a Dox-induced cardiomyopathy model. Given that ferroptosis has recently been found to play a dominant role in Dox-induced cardiomyopathy[7,36], we measured some recognized biomarkers for ferroptosis. Excessive ROS production and iron and lipotoxicity dependency are three hallmarks of ferroptosis. Indeed,

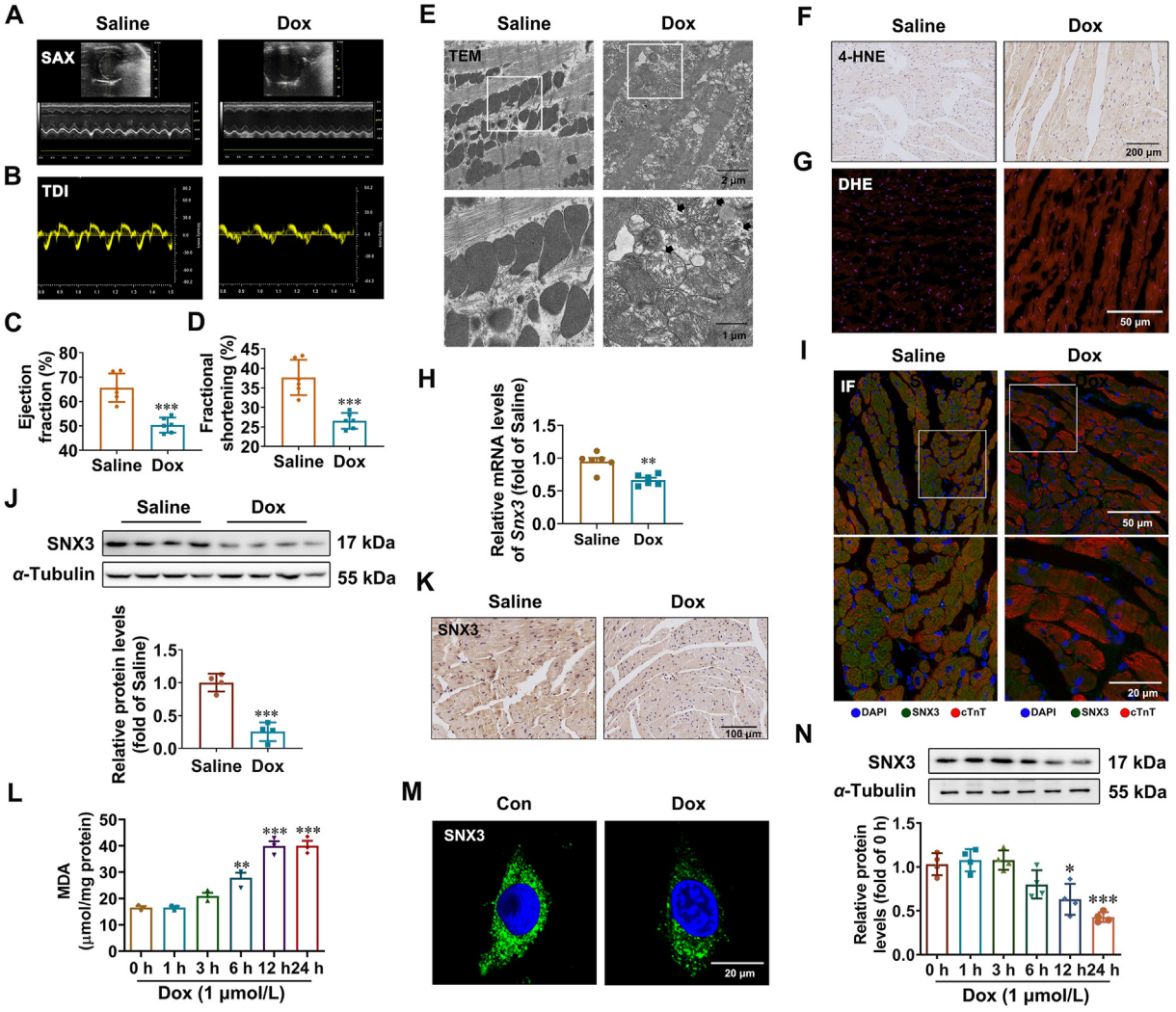

Figure 1 SNX3 expression is downregulated in Dox-induced cardiomyopathy. (A, B) Male C57BL/6 mice were i.p. injected with an accumulation dose of 24 mg/kg Dox or the equivalent volume of saline three times (on Days 1, 4, and 7, respectively). At the end of the trial, the mice were tested for cardiac function by echocardiography, and representative echocardiograms are presented. (C, D) The LV trace EF% and LV trace FS% were calculated. (E) Representative transmission electron microscopy images (scale bar: 1 μm) of heart tissue in control and Dox-treated mice. (F, G) 4-HNE IHC dyeing (scale bar: 200 μm) and DHE staining (scale bar: 50 μm) stained cross-sections of heart tissues are shown. (H) *Snx3* mRNA expression was detected by qPCR. (I) Representative IF images of SNX3 and cTnT staining (scale bar: 20 μm) in myocardial tissues from Dox-treated and saline-treated mice. (J, K) The protein expression of SNX3 in hearts from Dox-treated and saline-treated mice was analyzed by Western blotting and IHC staining (scale bar: 100 μm). (L) The level of MDA in NRCMs treated with 1 μmol/L Dox for 1, 3, 6, 12, and 24 h. (M, N) The protein expression of SNX3 in NRCMs treated with Dox (1 μmol/L) was measured by IF assay (scale bar: 20 μm) and Western blotting. Typical pictures of five independent experiments are shown. The data are shown as the mean ± SEM, $n = 3-5$ for cell test, $n = 6-9$ for mouse test. $^*P < 0.05$, $^{**}P < 0.01$, $^{***}P < 0.001$, $^{****}P < 0.0001$ *vs*. Con or Saline group. See also Figs. S1 and S2.

we observed severe distortion and enlargement of myocardial mitochondria (Fig. 1E), which are early indicators of ferroptosis[6,7]. Moreover, we observed Dox-induced ferroptosis *in vivo*, as shown by upregulated levels of lipid peroxidation-derived 4-hydroxynonenal (4-HNE) (Fig. 1F) and MDA (Fig. S1K), increased oxidative stress dyed with DHE dye (Fig. 1G). Notably, the mRNA and protein levels of SNX3 were remarkably decreased in the hearts of Dox-treated mice compared to control mice (Fig. 1H−K, Fig. S1L and S1M).

Since the death of terminally differentiated myocardial cells is well characterized in Dox-induced cardiomyopathy[37], the cell viability was examined after Dox treatment. As expected, the cell viability decreased up to 50% after 12 h of Dox (1 μmol/L) treatment (Supporting Information Fig. S2A). Mitochondrial injury was also observed in the Dox group, as implied by a decline in mitochondrial membrane potential (Fig. S2B) and mitochondrial matrix swelling or disorganization (Fig. S2C). Ferroptosis in Dox-treated cardiomyocytes was confirmed by the elevated intracellular Fe^{2+} level by a fluorescent probe, FerroOrange (Fig. S2D), as well as increased lipid ROS (Fig. S2E) and accumulated MDA content (Fig. 1L). The results of hoechst staining and flow cytometry suggest that apoptosis may exist in Dox-induced cardiomyopathy (Fig. S2F and S2G). In contrast, pyroptosis and necroptosis were not found in this model (Fig. S2H and S2I). Besides, we carried out bright field observation of cell morphology and the CCK8 assay to determine the cell viability in response to Dox treatment with or without various inhibitors of cell death. As shown in Fig. S2J and S2K, the ferroptosis inhibitor Fer-1 and iron chelator DFO both blocked Dox-induced cardiomyocyte mortality significantly. The inhibitors of pyroptosis (Ac-YVAD-CMK), apoptosis (Z-VAD-FMK) and necrosis (Necrosulfonamide) can reduce cell death caused by Dox treatment to varying degrees, but are not nearly as effective as ferroptosis inhibitors. The severe distortion and enlargement of myocardial mitochondria caused by Dox was mitigated by DFO (Fig. S2L). Our findings suggest that ferroptosis, rather than other types of PCD, was the primary cause of Dox-induced mortality in this model. Additionally, we further analyzed SNX3 expression in Dox treatment NRCMs. Consistent with the results obtained in mice, the mRNA and protein expression of SNX3 were also markedly reduced in Dox-treated NRCMs (Fig. 1M and N, Fig. S2M). Taken together, these findings suggest that SNX3 expression was associated with the development of Dox-induced ferroptosis and cardiomyopathy both *in vivo* and *in vitro*.

3.2. *Deletion of cardiac Snx3 attenuated Dox-induced cardiomyopathy by inhibition of ferroptosis in mouse model*

To test whether SNX3 deficiency attenuates to Dox-induced ferroptosis and cardiomyopathy, *Snx3*-cKO mice was generated and used as previously described[34]. The heart function of *Snx3*-cKO mice treated with Dox was evaluated (an accumulative dose of 24 mg/kg, i.p.) (Fig. 2A). SNX3 protein was barely detectable in the myocardial tissues of *Snx3*-cKO mice (Fig. 2B and C), confirming successfully deletion of myocardial SNX3 in *Snx3*-cKO mice. By using Perl staining, we observed increased iron levels in Dox-treated CTL mice, whereas there was no significant change in *Snx3*-cKO mice treated with Dox (Supporting Information Fig. S3A). In addition, decreased ROS production was also observed in *Snx3*-cKO mice treated with Dox compared with control mice, as evidenced by DHE staining of frozen heart slides (Fig. 2D, Fig. S3B). Furthermore, we found that the cardiac lipid peroxidation levels (4-HNE and MDA content) in Dox-treated CTL mice were much higher than those of saline-treated mice. However, Dox treatment failed to robustly induce lipid peroxidation in *Snx3*-cKO mice (Fig. 2E, Fig. S3C). In line with these findings, the myocardial tissues in the Dox group had significantly reduced mitochondrial membrane potential and increased mitochondrial atrophy and membrane density, but SNX3 deficiency relieved these Dox-induced effects (Fig. 2F, Fig. S3D).

As predicted, Dox treatment remarkably induced myocyte fibrosis and tissue disturbance in CTL mice relative to the saline group by histological staining (Fig. 2G, Supporting Information Fig. S4A). The hearts of Dox-treated CTL mice exhibited disorganization of myocytes, which was substantially ameliorated in those of *Snx3*-cKO mice (Fig. S4A). PSR staining revealed less cardiac fibrosis in *Snx3*-cKO mice than in CTL mice (Fig. 2G, Fig. S4B). In addition, the echocardiography results also showed myocardial injury by Dox, which induced the dilation of left ventricular (Fig. 2H−J, Fig. S3C−S3G). Compared with the CTL + saline group, the ejection fraction (Fig. 2K) and fractional shortening (Fig. S3E) of the Dox model group declined significantly, indicating a decline in cardiac function in Dox-treated mice. Notably, these responses of Dox-induced heart dysfunction were markedly reduced in *Snx3*-cKO mice (Fig. 2I and J, Fig. S4C and S4D). While there was no statistically significant difference in fractional shortening (Fig. S3E) or interventricular septum among the groups (Fig. S4F and S4G), the improvement in heart function in the *Snx*3-cKO group was apparent. Together, these data demonstrate that cardiac SNX3 deficiency significantly attenuated Dox-induced ferroptosis and cardiomyopathy in mice.

3.3. *Dox-induced cardiomyopathy and ferroptosis were aggravated in cardiac-specific Snx3 transgenic mice*

To further investigate whether SNX3 contributes to Dox-induced cardiomyopathy, *Snx3*-cTg mice, which were generated as we previously described[34], were treated with Dox (Fig. 3A). SNX3 was successfully overexpressed in the cardiac tissue of *Snx3*-cTg mice, as evidenced by Western blotting (Fig. 3B) and immunohistochemistry analysis (Fig. 3C). We further examined the effect of SNX3 overexpression on ferroptosis in Dox-induced cardiomyopathy *in vivo*. SNX3 overexpression exacerbated the Dox-induced ROS accumulation (Fig. 3D). Next, JC-1 staining showed remarkably decreased mitochondrial membrane potential in the hearts of *Snx3*-cTg mice compared to those of non-transgenic (N-Tg) mice (Supporting Information Fig. S5A), and the hearts of *Snx3*-cTg mice showed mitochondrial atrophy and increased membrane density (Fig. 3E). Ferroptosis induction in cardiac tissue was confirmed by the elevated intracellular Fe^{2+} level and total Fe by an Iron Assay Kit, which indicated that SNX3 overexpression significantly exacerbated Dox-induced accumulation of Fe^{2+} or total Fe in cardiac tissues (Fig. 3F and G, Fig. S5B). As shown in Fig. 3H and I, SNX3 overexpression significantly elevated cardiac MDA and 4-HNE content, mimicking the effects of Dox stimulation. Furthermore, our data also demonstrate a significant trend toward an increase in cardiac 4-HNE in the SNX3 overexpression plus Dox treatment group compared with Dox treatment alone.

Histological staining showed that SNX3 overexpression significantly caused myocardial arrangement disorders and cardiac fibrosis in mice (Fig. 3J−L, Supporting Information Fig. S6A). Furthermore, we tested whether SNX3 overexpression exacerbates

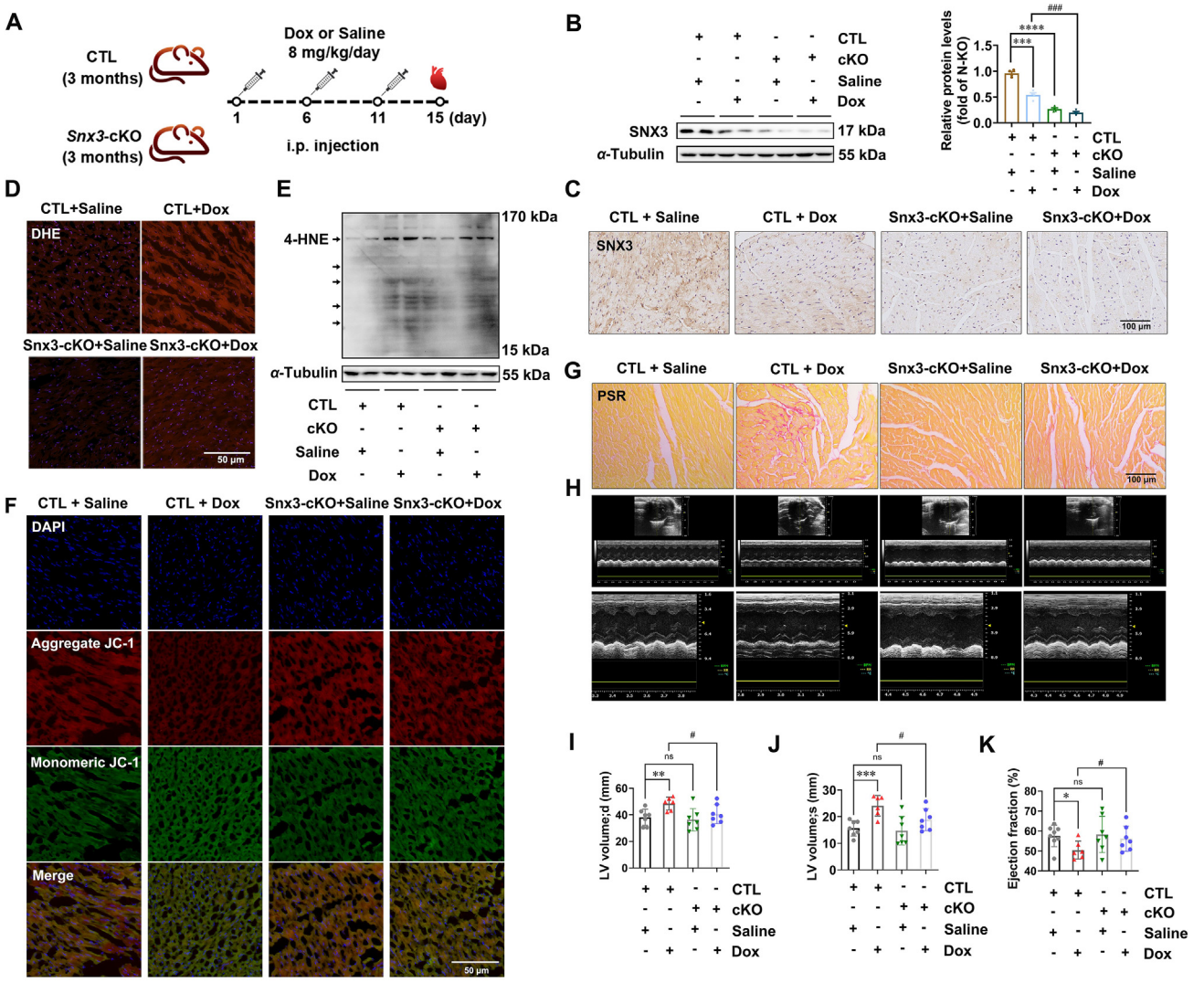

Figure 2 Deletion of cardiac Snx3 attenuates Dox-induced cardiomyopathy by inhibiting ferroptosis in mouse model. *Snx3*-cKO mice and their respective CTL *mice* were i.p. injected with an cumulative dose of 24 mg/kg Dox or an equivalent amount of sterile normal saline three times (on Days 1, 6, and 11, respectively). (A) Schematic illustration of Dox administration in animals in 4 groups: male *Snx3*-cKO or CTL mice at 3 months were i.p. injected with Dox or saline. (B, C) Western blotting and IHC assays (scale bar: 100 μm) were used to evaluate SNX3 protein expression. (D) DHE dye (scale bar: 50 μm) stained frozen heart slides are shown. (E) The lipid peroxidation level in hearts was assessed by measuring 4-HNE. (F) Typical pictures of cardiac by JC-1 dyeing (scale bar: 50 μm) in frozen heart slides. (G) PSR staining (scale bar: 100 μm) stained cross-sections of heart tissues. (H) Typical echocardiograms were offered. (I−K) Echocardiographic parameters, including ejection fraction and LV end-systolic/end-diastolic volume. Typical pictures of five independent experiments are shown. The data are shown as the mean ± SEM, $n = 6-9$. $^{*}P < 0.05$, $^{**}P < 0.01$, $^{***}P < 0.001$, $^{****}P < 0.0001$ *vs*. CTL + saline group; $^{\#}P < 0.05$, $^{\#\#}P < 0.01$, $^{\#\#\#}P < 0.001$, $^{\#\#\#\#}P < 0.0001$ *vs*. CTL + Dox group. See also Figs. S3 and S4.

Dox-induced cardiomyopathy. Similar to the results obtained with Dox treatment, SNX3 overexpression also resulted in severe myocardial injury, as indicated by echocardiography results (Fig. 3M), including the decline in ejection fraction (Fig. 3N), fractional shortening (Fig. 3O), cardiac output (Fig. S6B) and stroke volume (Fig. S6C), as well as an increase in end-systolic/end-diastolic LV volume (Fig. 3P, Fig. S6D). In addition, the hearts of Dox-treated *Snx3*-cTg mice showed a lower ejection fraction (Fig. 3N) and fractional shortening (Fig. 3O) than those of Dox-treated N-Tg mice, indicating that SNX3 overexpression was associated with reduced cardiac contractile function in Dox-treated mice, although the difference in some echocardiographic parameters did not reach statistical significance (Fig. S6B−S6D). Collectively, these findings indicate that *Snx3*-cTg mice were more sensitive to Dox-induced ferroptosis and myocardial injury.

3.4. SNX3 exacerbated Dox-induced cardiomyopathy by inducing ferroptosis in cardiomyocytes

We next carried out experiments *in vitro* to further corroborate the role of SNX3 in the progression of Dox-induced cardiomyopathy. NRCMs were infected with Ad-shSNX3 or Ad-SNX3 before Dox treatment. The knockdown or overexpression of SNX3 was verified at the protein level by Western blotting (Supporting Information Fig. S7A and S7B). The effects of SNX3 on cell viability were also examined by CCK8 analysis (Fig. S7C and S7D);

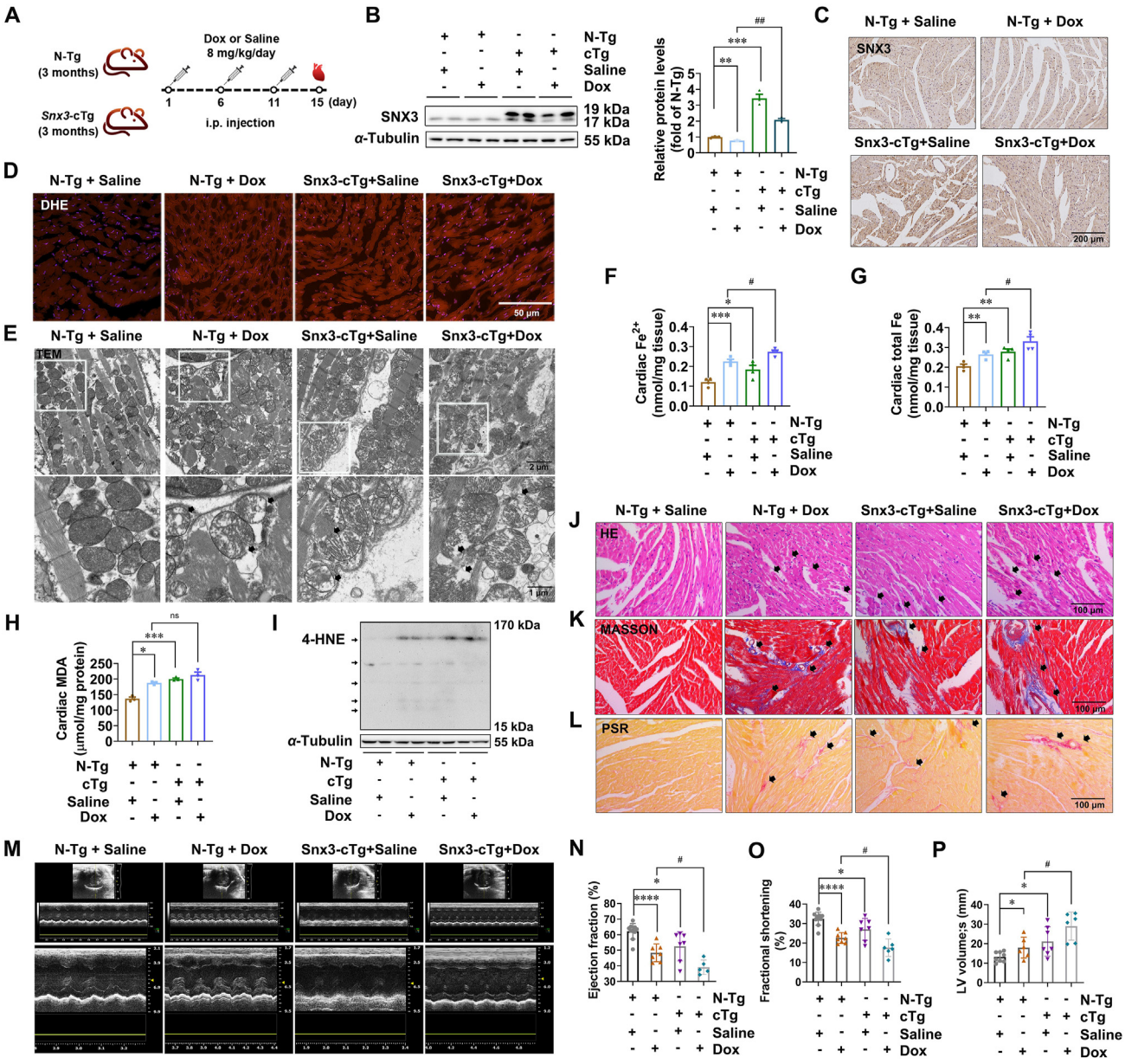

Figure 3 Cardiac-specific Snx3 transgene aggravates Dox-induced ferroptosis and cardiomyopathy in mice. *Snx3*-cTg mice and their respective N-Tg mice were i.p. injected with an accumulative dose of 24 mg/kg Dox or an equivalent amount of sterile normal saline three times (on Days 1, 6 and 11, respectively). (A) Schematic illustration of Dox administration in animals in 4 groups: male *Snx3*-cTg or N-Tg mice at 3 months were i.p. injected with Dox or saline. (B, C) Western blotting and IHC assays (scale bar: 200 μm) were used to examine the protein level of SNX3. (D) DHE staining (scale bar: 50 μm) is shown. (E) Transmission electron microscopy of heart tissues (scale bar: 1 μm). (F, G) The Iron Assay Kit indicated the Fe^{2+} and total Fe contents of cardiac tissues. (H) The lipid peroxidation level in hearts was assessed by measuring MDA levels. (I) Western blot analysis for 4-HNE in heart tissue. (J−L) HE staining, Masson's trichrome staining, and PSR staining (scale bar: 100 μm) are shown. (M) Representative echocardiography is shown. (N−P) The echocardiographic parameters were measured, including ejection fraction, fractional shortening and LV end-systolic volume. Typical pictures of five independent experiments are shown. The data are shown as the mean ± SEM, $n = 6$−9. $^{*}P < 0.05$, $^{**}P < 0.01$, $^{***}P < 0.001$, $^{****}P < 0.0001$ *vs*. N-Tg + Saline group; $^{\#}P < 0.05$, $^{\#\#}P < 0.01$, $^{\#\#\#}P < 0.001$, $^{\#\#\#\#}P < 0.0001$ *vs*. N-Tg + Dox group. See also Figs. S5 and S6.

interestingly, SNX3 exacerbated Dox-induced cell death (Fig. S7D). To further investigate the potential role of ferroptosis in SNX3-mediated exacerbation of Dox-induced cell death, we detected intracellular lipid ROS levels, and the results revealed that SNX3 overexpression enhanced intracellular lipid peroxidation, whereas no such changes in knockdown SNX3 with Dox-treatment are apparent (Fig. 4A−C, Fig. S7E). In addition, we found that SNX3 overexpression led to noticeably increased fluorescence intensity of FerroOrange in NRCMs, similar to Dox treatment. Whereas, SNX3 deficiency relieved these Dox-induced effects (Fig. 4D, Fig. S7F). As shown in Fig. 4E and Fig. S7G, SNX3 overexpression resulted in shrunken and ruptured mitochondria, and Mito Tracker Red staining was consistent with the TEM results (Fig. 4F, Fig. S7H). We also detected intracellular

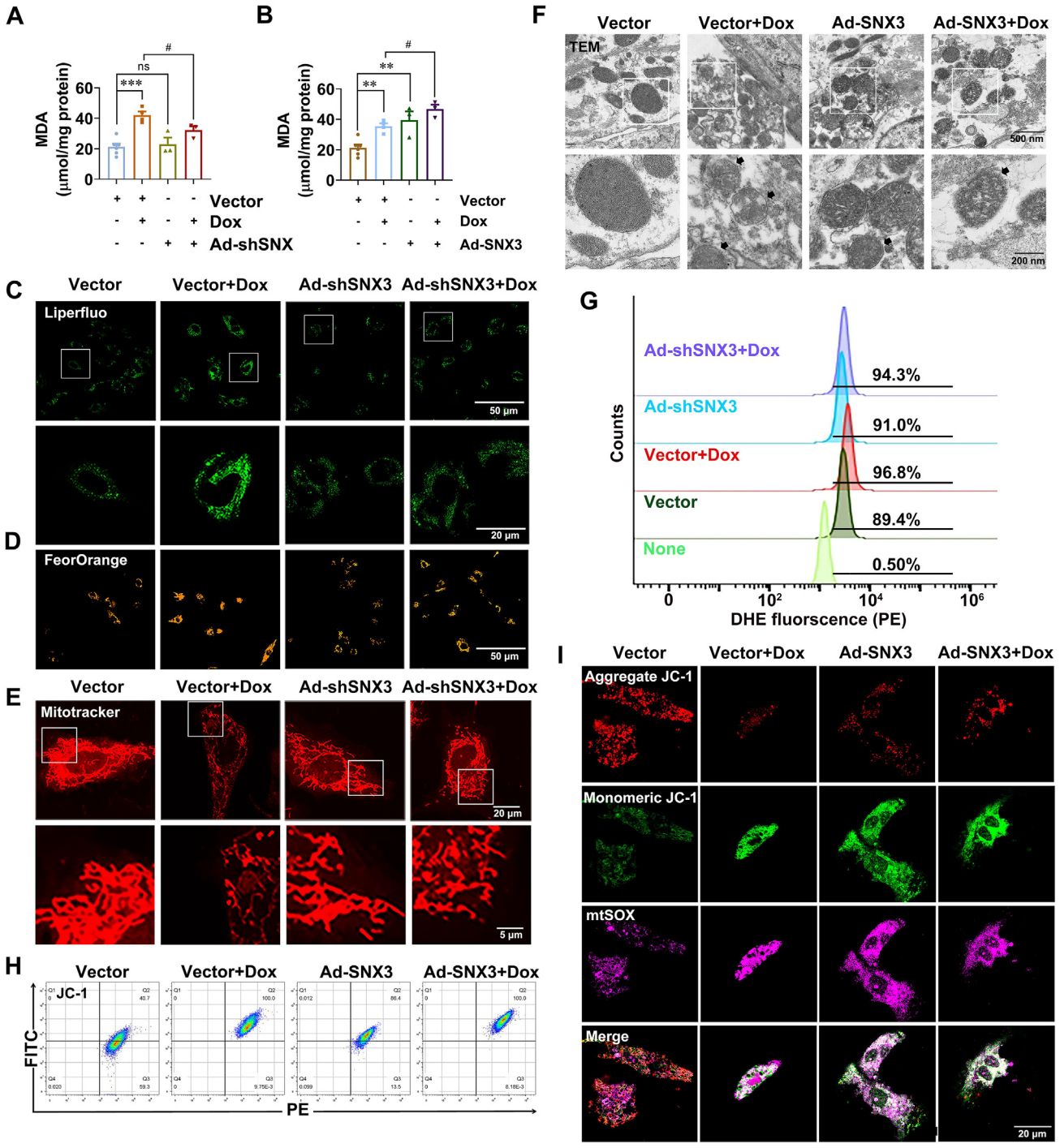

Figure 4 SNX3 mediated ferroptosis in NRCMs. NRCMs were pre-infected with Ad-shSNX3 or Ad-SNX3 for 36 h and then were treated with Dox (1 μmol/L) for an extra 12 h in the presence of Ad-shSNX3 or Ad-SNX3. (A, B) The intracellular MDA was assayed by the kit. (C−F) Liperfluo dyeing (scale bar: 50 μm) for intracellular lipid peroxidation; FerroOrange dyeing (scale bar: 50 μm) for intracellular Fe^{2+}; Mitotracker-red staining (scale bar: 5 μm) for mitochondrial morphology; Representative TEM mitochondria images of NRCMs (scale bar: 200 nm). (G, H) Flow cytometry assay for mitochondrial membrane potential using DHE and JC-1. (I) Representative images of NRCMs were live stained with JC-1 dyes and MitoSox (scale bar: 20 μm) for MitoROS. The typical pictures from five independent experiments were offered. The data are showed as the mean ± SEM, $n = 3-5$. $^{*}P < 0.05$, $^{**}P < 0.01$, $^{***}P < 0.001$, $^{****}P < 0.0001$ *vs.* Vector group; $^{\#}P < 0.05$, $^{\#\#}P < 0.01$, $^{\#\#\#}P < 0.001$, $^{\#\#\#\#}P < 0.0001$ *vs.* Vector + Dox group. See also Fig. S7.

total ROS with DHE staining by flow cytometry analysis, and the results showed that SNX3 overexpression caused an increase in total intracellular ROS levels (Fig. 4G, Fig. S7I). To assess the impact of SNX3 on mitochondrial fitness, we measured mitochondrial membrane potential and superoxide production with JC-1 and MitoSOX. Ad-SNX3-infected NRCMs had lower mitochondrial membrane potentials (Fig. 4H and I, Fig. S7J and S7K) and markedly elevated generation of mitochondrial

superoxide (Fig. 4I, Fig. S7L). Western blotting analysis of four ferroptosis biomarkers revealed that SNX3 overexpression mimicked the effects of Dox on downregulating the expression of SLC7A11, FTH1, GPX4 while upregulating the expression of COX2 in the hearts of N-Tg mice (Fig. S7M). Besides, the effect of SNX3 on other cell death types was investigated by detecting their markers. Expression of pyroptosis-related proteins such as Caspase-1 and GSDMD-N were not changed by Dox treatment or SNX3 overexpression (Fig. S7N). SNX3 slightly increased the protein levels of C-caspase 3 and pS358-MLKL (Fig. S7O−S7Q), which are markers of apoptosis and necrosis, respectively. Moreover, the CCK8 assay to determine ferroptosis, rather than other types of PCD, was the primary cause of SNX3-induced mortality in this model (Fig. S7R). Collectively, these results suggest that multiple cell death patterns may coexist in the SNX3-mediated exacerbation of Dox-induced cell death, cardiac-specific SNX3 overexpression exacerbated ferroptosis, while SNX3 deficiency attenuated Dox-induced ferroptosis *in vitro*, corroborating the *in vivo* evidence.

Erastin was recognized as a classical inducer for regulating PCD[38] and served as a positive control. As expected, we noted that erastin treatment significantly triggered NRCM ferroptosis characterized by increased free Fe^{2+} content and lipid peroxidation products (Supporting Information Fig. S8A and S8B), severely disrupted mitochondrial cristae and compromised membranes (Fig. S8C), and decreased mitochondrial membrane potential and cell viability (Fig. S8D and S8E). Interestingly, SNX3 knockdown was unable to alleviate erastin-induced ferroptosis in NRCMs (Fig. S8). Furthermore, we determined the effect of SNX3 ablation in NRCMs in response to erastin treatment; our data showed that SNX3-loss significantly reduced iron content and lipid peroxidation products following Dox treatment. Notably, the protective effect of Ad-shSNX3 on ferroptosis in Dox-treated NRCMs was abolished by the ferroptosis activator erastin, as indicated by the FerroOrange assay and MDA measurement (Fig. 5A and B), as well as TEM and JC-1 or DHE staining (Fig. 5C and D, Fig. S8F), implying a critical role of ferroptosis inhibition in SNX3 deletion-mediated myocardial protection in Dox-induced cardiomyopathy *in vitro*.

To further investigate the contribution of ferroptosis to cardiomyopathy during the SNX3-induced Dox injury process, two small molecule ferroptosis inhibitors were used, DFO, which is an iron chelator, and Fer-1, which is a lipid radical scavenger, to treat NRCMs at the indicated concentrations and times, respectively. Accordingly, our analysis revealed that the Fe^{2+} content and lipid peroxidation products were severely accumulated and cell viability was decreased in Dox-treated NRCMs, while these Dox-induced outcomes were rescued by both DFO and Fer-1 therapy (Supporting Information Fig. S9A−S9D). Surprisingly, we found that mitochondrial morphology was severely distorted and enlarged upon infection of NRCMs with Ad-SNX3 infection, and these effects were largely reversed by treatment with the ferroptosis inhibitor DFO (Fig. 5E and F, Fig. S9E). Moreover, we further observed that SNX3 overexpression induced the enhancement of intracellular Fe^{2+} and lipid peroxidation products, which were reversed by the ferroptosis inhibitor DFO or Fer-1. The effect of DFO was more pronounced than Fer-1 (Fig. 5G−I). In addition, Fer-1 reduced the intracellular accumulation of lipid peroxidation or total ROS in NRCMs infected with Ad-SNX3 by performing Liperfluo and DHE staining. Similar results were obtained with DFO treatment (Fig. S9F and S9G). Taken together, our data strongly supported that SNX3 exacerbated Dox-induced cardiomyopathy *via* the induction of ferroptosis.

3.5. *Forced expression of cardiac-specific Snx3 aggravated Dox-induced cardiomyopathy by inducing ferroptosis*

Our current results show that SNX3 aggravated Dox-induced cardiomyopathy in mice and that overexpression of SNX3 induced ferroptosis both *in vitro* and *in vivo*. We next tested whether ferroptosis was involved in SNX3-induced Dox injury. *Snx3*-cTg mice were i.p. injected with DFO (100 mg/kg) before Dox treatment (Fig. 6A). In *Snx3*-cTg mice after Dox treatment, the total ROS production in frozen heart slides significantly increased (Fig. 6B, Supporting Information Fig. S10A), as did the iron level in the heart by the Iron Assay Kit (Fig. 6C and D, Fig. S10B) and Perl staining (Fig. S10C). Interestingly, these effects were reversed by treatment with DFO. Besides, we noticed that DFO treatment also attenuated Dox-induced increases in MDA and 4-HNE levels (Fig. 6E, Fig. S10D). In addition, TEM results showed severely distorted and enlarged myocardial mitochondria in Dox-treated *Snx3*-cTg mice, and these SNX3 plus Dox-induced effects were rescued by DFO treatment (Fig. 6F, Fig. S10E). Moreover, Dox reduced the ejection fraction, fractional shortening, cardiac output, left ventricular end-systolic volume, and MV E'/A' ratio in *Snx3*-cTg mice, was improved by DFO treatment in *Snx3*-cTg mice (Fig. 6G−L, Fig. S10F−S10I). Consistently, compared with mice treated with Dox alone, mice pretreated with DFO had attenuated cardiac ferroptosis (Fig. S10A−S10D). In summary, DFO treatment reduced myocardial ferroptosis in Dox-induced mice (Fig. 6, Fig. S10). Taken together, our data strongly support that SNX3 exacerbates Dox-induced cardiomyopathy *via* the induction of ferroptosis.

3.6. *SNX3 facilitated TFRC recycling by directly interacting to trigger ferroptosis*

Our results showed that SNX3 served as a positive regulator of ferroptosis in Dox-induced cardiomyopathy which prompted us to investigate its underlying mechanisms. TFRC, which couples with the complex of transferrin and Fe^{3+} on the PM and subsequently translocate to cytoplasm, is considered a pivotal endogenous regulator of iron homeostasis[39,40]. Co-IP assay and His-tag-pull-down analysis were further utilized to evaluate protein interactions. Indeed, the co-IP experiment confirmed that SNX3 interacted with TFRC in NRCMs (Fig. 7A), and the *in vitro* protein binding assay identified the interaction between TFRC and SNX3-His protein (Fig. 7B). Moreover, we applied the PLA assay to quantify the location of TFRC in SNX3 binding, which examined the binding position of SNX3 to endogenous TFRC *via* PLA positive signals. We observed that the PLA-positive signals were mainly near the cell membrane and in the cytoplasm (Fig. 7C). In addition, IF staining was consistent with the PLA results (Fig. 7D). Besides, SNX3 knockdown inhibited the increase of Dox-induced TFRC protein (Fig. 7E and F); SNX3 overexpression markedly increased the protein levels of TFRC (Fig. 7G, Supporting Information Fig. S11A).

TFRC (in red) was found colocalized with LAMP1 (a marker of lysosomes in green) by laser scanning confocal analysis, suggesting that TFRC protein is localized in lysosomes (Fig. S11B). The protein levels of TFRC in lysosomes were increased by SNX3 knockdown, but inhibited by SNX3 overexpression (Fig. S11B). Besides, chloroquine, a lysosome inhibitor, reversed the reduction

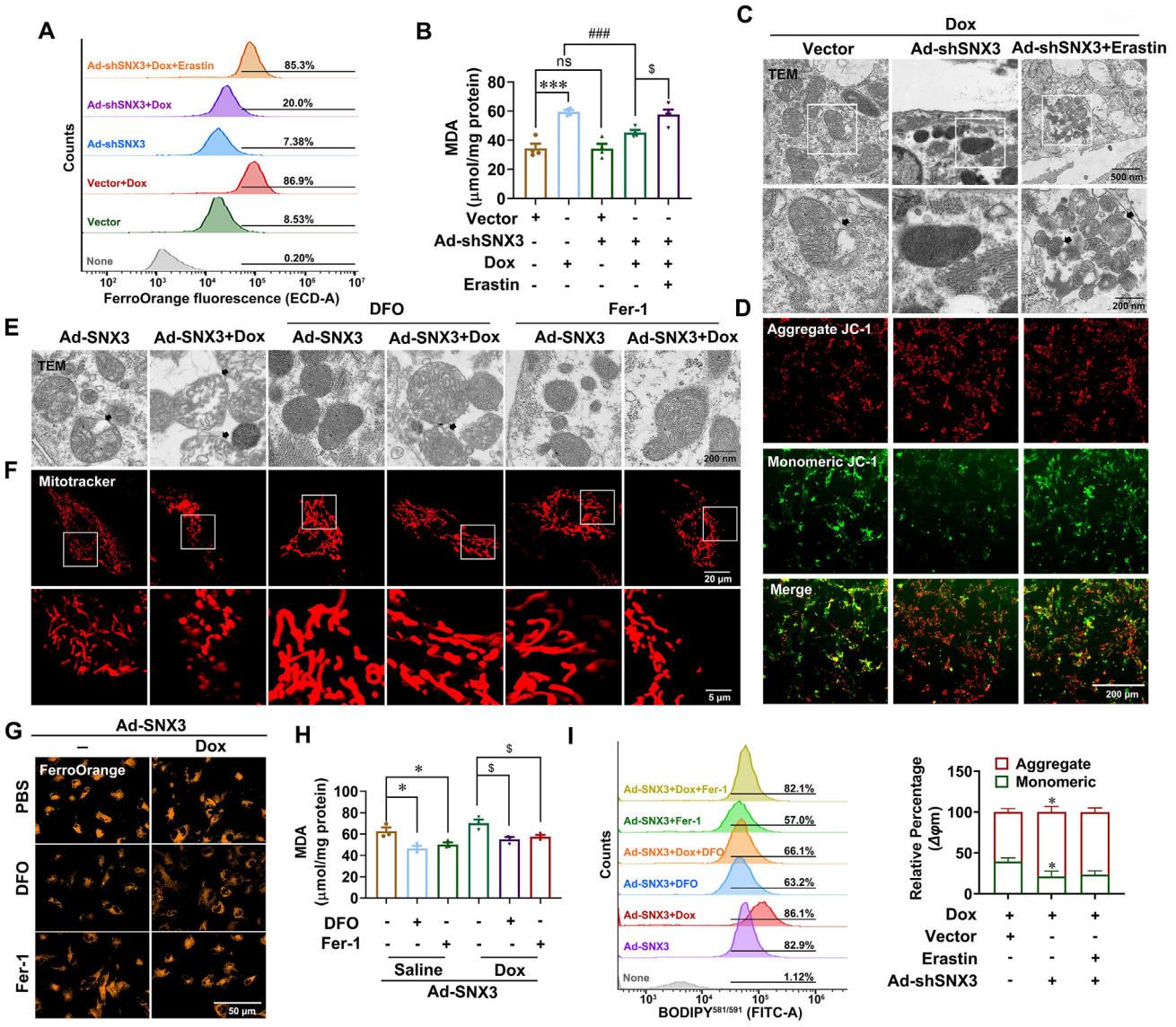

Figure 5 SNX3 exacerbated Dox-induced cardiomyopathy by promoting ferroptosis in NRCMs. NRCMs were preinfected with Ad-shSNX3 or Ad-SNX3 for 36 h and then treated with Dox (1 μmol/L) for an additional 12 h and Fer-1 (3 μmol/L) or DFO (100 μmol/L) or erastin (10 μmol/L) for an additional 24 h in the presence of Ad-shSNX3 or Ad-SNX3. (A) Measurement of intracellular Fe^{2+} levels by flow cytometry using FerroOrange. (B) A MDA assay kit was used to assay intracellular MDA. (C, D) Representative images of TEM mitochondria (scale bar: 200 nm) and JC-1 staining in NRCMs (scale bar: 200 μm). (E, F) Representative mitochondrial morphology images by TEM analysis (scale bar: 200 nm) and Mito Tracker Red staining (scale bar: 5 μm). (G) FerroOrange dyeing (scale bar: 50 μm) for intracellular Fe^{2+}. (H, I) The lipid peroxidation level in NRCMs was measured by an MDA assay kit and analyzed by flow cytometry using C11-BODIPY$^{581/591}$. Typical pictures of five independent experiments are shown. The data are shown as the mean ± SEM, $n = 3-5$ for the cell test. $^{*}P < 0.05$, $^{**}P < 0.01$, $^{***}P < 0.001$, $^{****}P < 0.0001$ *vs.* Vector group; $^{\#}P < 0.05$, $^{\#\#}P < 0.01$, $^{\#\#\#}P < 0.001$, $^{\#\#\#\#}P < 0.0001$ *vs.* Vector + Dox group. See also Figs. S8 and S9.

in TFRC protein levels caused by SNX3 silencing (Fig. S11C). These results suggest that SNX3 may regulate the trafficking of the cargo protein TFRC to avoid its degradation by lysosomes. Furthermore, the protein level of TFRC in PM were significantly increased by overexpression of SNX3 (Fig. 7H and I, Fig. S11D). Conversely, knocking down SNX3 will reduce the TFRC content in the PM (Fig. 7H and I). These results suggest that SNX3 rescued TFRC from the lysosomal degradation pathway and transported it to PM.

Next, we asked whether TFRC was involved in SNX3-induced ferroptosis. AAV9 vectors carrying either sh-TFRC or sh-NC were delivered to LV of *Snx3*-cTg mice by intramyocardial injection. Successful delivery of sh-TFRC and sh-NC into the mouse myocardium was verified by the appreciable presence in myocardial sections of fluorescence signal elicited by GFP (Supporting Information Fig. S12A). And the knockdown efficiency of *Tfrc* in mouse myocardial tissue was verified by qPCR (Fig. S12B). Ferroptosis in cardiac tissue of *Snx3*-cTg mice was revealed by the elevated intracellular Fe^{2+} level and total Fe (Fig. 8A, Fig. S12C). However, the cardiac iron accumulation and lipid peroxidation MDA content induced by SNX3 overexpression was significantly inhibited after TFRC silencing (Fig. S12D). In

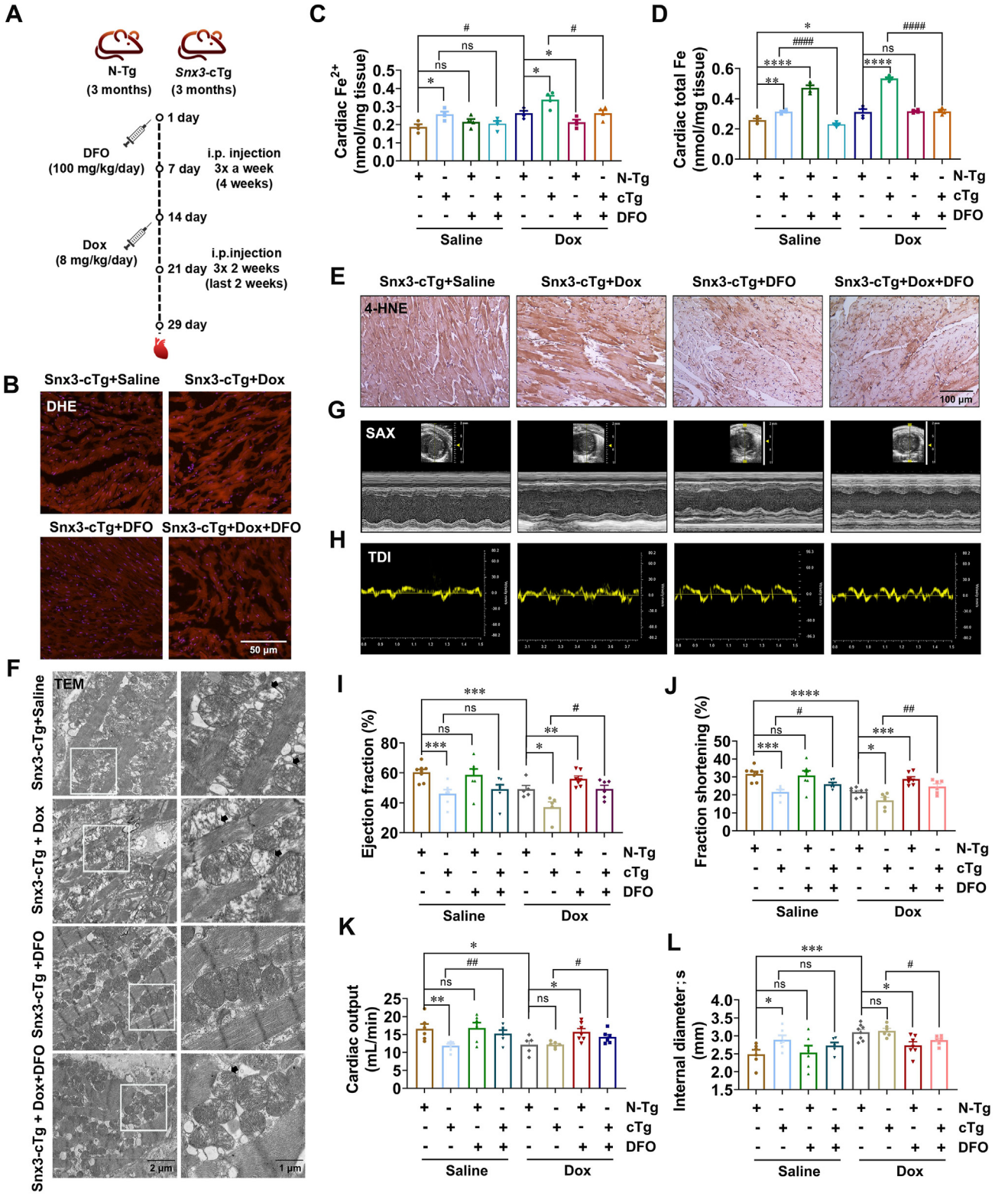

Figure 6 Forced expression of cardiac-specific Snx3 aggravates Dox-induced cardiomyopathy by inducing ferroptosis. *Snx3*-cTg mice were i.p. injected with DFO (100 mg/kg) or the corresponding vehicle (15% castor oil) thrice a week for 4 weeks. Three weeks after DFO therapy, the animals were randomized and assigned to receive an cumulative dose of 24 mg/kg Dox or the same volume of saline for the last week. Mice were anesthetized using echocardiography 3 days after the Dox remedy. In addition, NRCMs were preinfected with Ad-shSNX3 or Ad-SNX3 for 36 h and then treated with Dox (1 μmol/L) for an additional 12 h and Fer-1 (3 μmol/L) or DFO (100 μmol/L) or erastin (10 μmol/L) for an additional 24 h in the presence of Ad-shSNX3 or Ad-SNX3. (A) Schematic illustration of DFO and Dox administration in animals in 8 groups: male *Snx3*-cTg or N-Tg mice at 3 months were i.p. injected DFO or the corresponding vehicle (15% castor oil) 3 weeks before Dox treatment. Three days

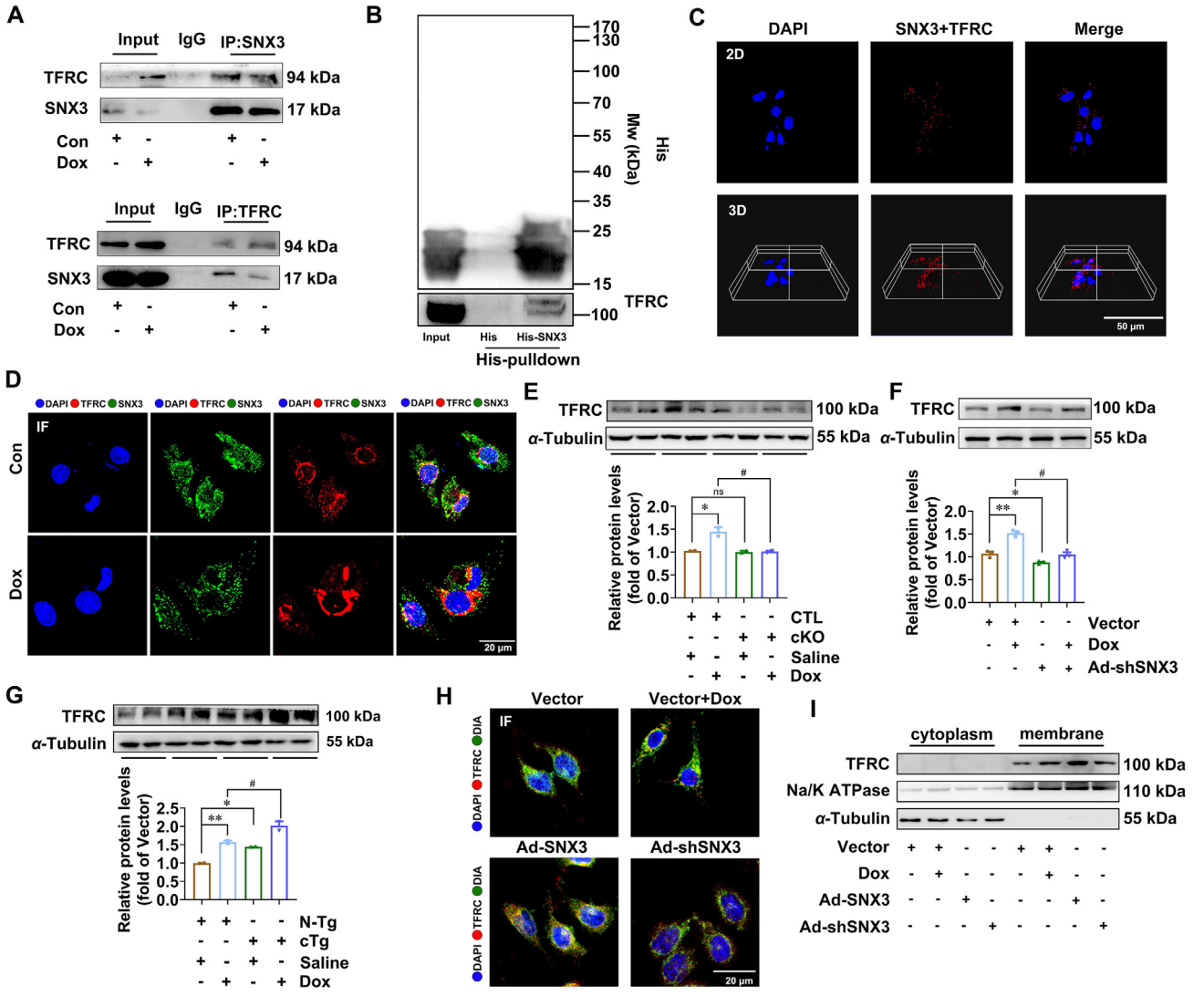

Figure 7 SNX3 facilitates the recycling of TFRC by direct interaction to trigger ferroptosis. NRCMs were preinfected with Ad-shSNX3 or Ad-SNX3 for 36 h and then treated with Dox (1 μmol/L) for an additional 12 h in the presence of Ad-shSNX3 or Ad-SNX3. Other groups of NRCMs were infected with Ad-SNX3 before transfecting siRNAs of siTFRC and were infected with Ad-shSNX3 before transfecting plasmids of TFRC. (A) NRCMs were infected with Ad-SNX3 and transfected with TFRC plasmid, and Co-IP was used to assess proteins. (B) His-SNX3 proteins induced with cell lysates of SNX3 or TFRC protein overexpressed by plasmid for 4 °C overnight and then added His-beads for incubation for 1 h at 37 °C, and immunoprecipitated proteins were examined according to Western Blotting. (C) PLA was observed by 3-dimensional projections. (D) Intracellular colocalization of SNX3 (green) and TFRC (red) was identified by confocal IF microscopy (scale bar: 20 μm). (E−G) Western blotting evaluated the protein expression of TFRC *in vivo* and *in vitro*, and IF analysis (scale bar: 20 μm) detected the TRFC protein levels in different treatment groups. (H) Intracellular colocalization of membrane probe DIA (green) and TFRC (red) was identified by confocal IF microscopy (scale bar: 20 μm). (I) Western blotting analyses of membrane and cytoplasm translocation of TFRC in NRCMs. Typical pictures of five independent experiments are shown. The data are shown as the mean ± SEM, $n = 6–9$ for the mouse test. $^{*}P < 0.05$, $^{**}P < 0.01$, $^{***}P < 0.001$, $^{****}P < 0.0001$ *vs.* N-Tg + Saline group or Vector group; $^{\#}P < 0.05$, $^{\#\#}P < 0.01$, $^{\#\#\#}P < 0.001$, $^{\#\#\#\#}P < 0.0001$ *vs.* *Snx3*-cTg + Saline group or Vector + Dox group. See also Fig. S11.

after Dox treatment, the mice were analyzed by echocardiography. (B) DHE staining (scale bar: 50 μm) is shown. (C, D) The Fe^{2+} and total Fe contents of the cardiac tissues. (E) 4-HNE IHC dyeing (scale bar: 100 μm) are shown. (F) Transmission electron microscopy of cardiac mitochondrial morphology (scale bar: 1 μm). (G, H) Representative echocardiography of the parasternal short-axis and tissue Doppler imaging are presented. (I−L) Ejection fraction, fractional shortening, cardiac output, and internal diameter were measured. Typical pictures of five independent experiments are shown. The data are shown as the mean ± SEM, $n = 6–9$ for the mouse test. $^{*}P < 0.05$, $^{**}P < 0.01$, $^{***}P < 0.001$, $^{****}P < 0.0001$ *vs.* N-Tg + Saline group or N-Tg + Dox group; $^{\#}P < 0.05$, $^{\#\#}P < 0.01$, $^{\#\#\#}P < 0.001$, $^{\#\#\#\#}P < 0.0001$ *vs.* *Snx3*-cTg + Saline group or *Snx3*-cTg + Dox group. See also Fig. S10.

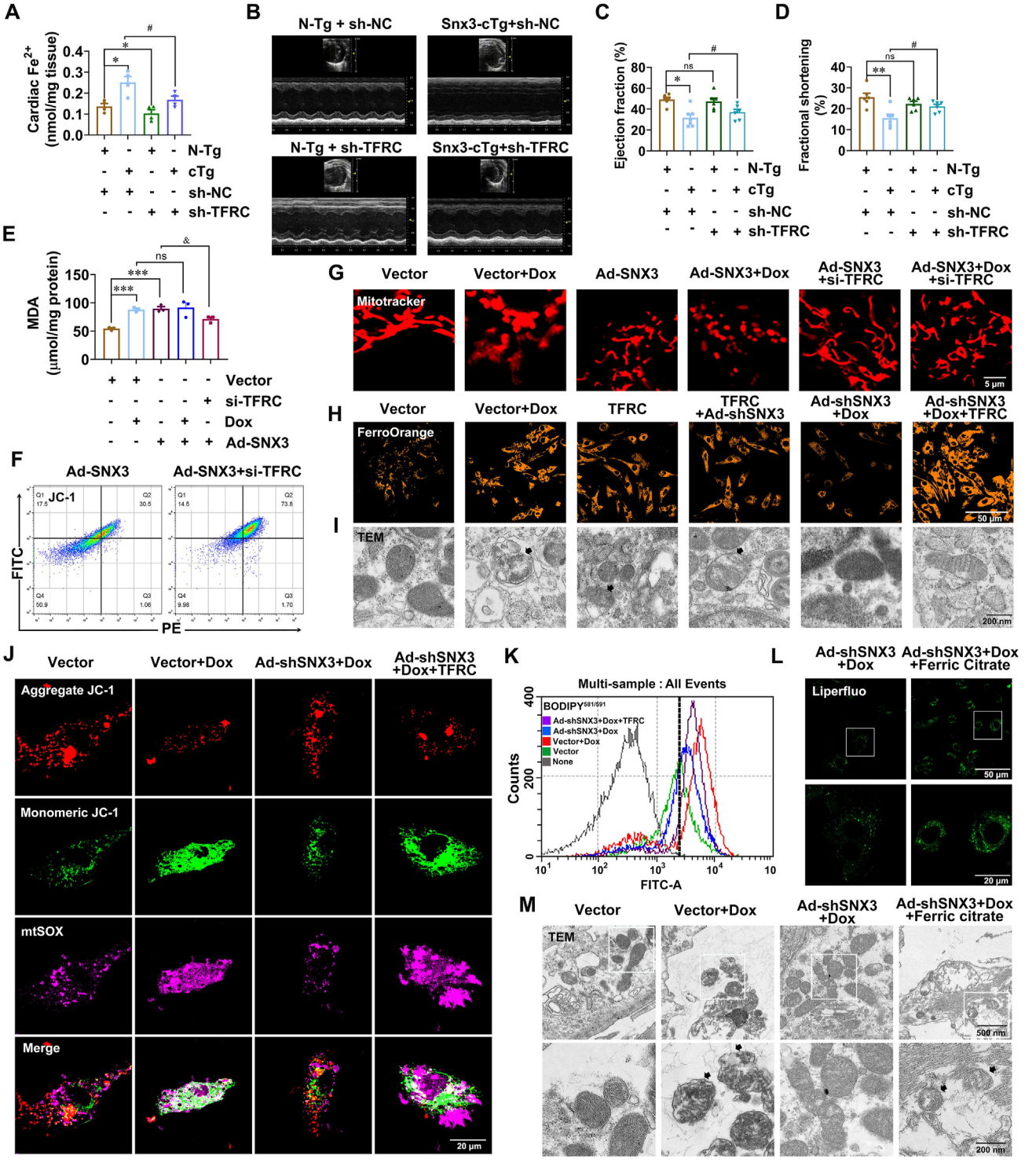

Figure 8 SNX3 exacerbates Dox-induced cardiomyopathy by promoting TFRC-dependent ferroptosis. *Snx3*-cTg mice were intramyocardially injected at three to five sites with sh-TFRC or an empty vector sh-NC at a dose of 10^{11} viral genome particles per mouse. Mice were anesthetized using echocardiography 4 week after the Advinjection. In addition, NRCMs were preinfected with Ad-shSNX3 or Ad-SNX3 for 36 h and then treated with Dox (1 μmol/L) for an additional 12 h in the presence of Ad-shSNX3 or Ad-SNX3. Other groups of NRCMs were infected with Ad-SNX3 before transfecting siRNAs of siTFRC and were infected with Ad-shSNX3 before transfecting plasmids of TFRC. In addition, another group of NRCMs was treated with Dox (1 μmol/L) and ferric citrate (100 μmol/L) for an additional 12 h in the presence of Ad-shSNX3. (A) The Fe^{2+} contents of the cardiac tissues. (B) Representative echocardiography is shown. (C, D) The echocardiographic parameters were measured, including ejection fraction and fractional shortening. (E) The MDA assay kit was used to detect lipid peroxidation in NRCMs. (F) Flow cytometry analysis for JC-1 staining. (G−I) Typical pictures of Mito Tracker Red dyeing (scale bar: 5 μm) and FerroOrange dyeing (scale bar: 50 μm) and TEM (scale bar: 200 nm). (J) Representative images of NRCMs were live stained with JC-1 dye for mitochondrial membrane potential and

line with these findings, the myocardial tissues in *Snx3*-cTg mice had significantly increased mitochondrial atrophy and membrane density, but TFRC deficiency relieved these SNX3-induced effects (Fig. S12E). Then, we investigated the effects of TFRC on cardiac function in *Snx3*-cTg mice. Both EF and FS were substantially lower in *Snx3*-cTg mice (Fig. 8B−D), compared with the N-Tg mice. As well as an increase in end-systolic LV volume in *Snx3*-cTg mice (Fig. S12F). Strikingly, in the *Snx3*-cTg mice that had received sh-TFRC for 4 weeks, the above mentioned parameters of cardiac function were all improved, the value of EF and FS nearly recovered back to normal levels (Fig. 8C and D, Fig. S12G).

We next carried out experiments *in vitro* to further corroborate the role of TFRC in the progression of SNX3 overexpression-induced ferroptosis (Fig. S12H−S12K). In Ad-SNX3-infected NRCMs, siRNA was used to knockdown *Tfrc*. We found that TFRC knockdown reduced the intracellular accumulation of lipid peroxidation products or free Fe^{2+} in Ad-SNX3-infected NRCMs (Fig. 8E, Fig. S12L). As expected, mitochondrial morphology was severely distorted, and mitochondrial membrane potential was reduced in NRCMs infected with Ad-SNX3. Notably, these effects were largely reversed by TFRC loss (Fig. 8F and G, Fig. S12M), indicating that SNX3 mediates ferroptosis *via* regulation of the TFRC pathway. To further corroborate these results, NRCMs were infected with Ad-shSNX3 followed by transfection with a TFRC plasmid. We found that the protective effect of Ad-shSNX3 on Dox-treated NRCMs against ferroptosis was eliminated by overexpression of TFRC, as evidenced by elevated MDA levels (Fig. S12N), increased free Fe^{2+} (Fig. 8H), severely distorted and enlarged myocardial mitochondria (Fig. 8I, Fig. S12O), significantly reduced mitochondrial membrane potential by flow cytometry analysis (Fig. 8F, Fig. S12R), markedly elevated generation of mitochondrial superoxide with JC-1 and MitoSOX costaining (Fig. 8J, Fig. S12P and S12Q), and increased lipid peroxidation products with C11-$BODIPY^{581/591}$ staining (Fig. 8K, Fig. S12S). Together, these findings indicated that SNX3 exacerbated ferroptosis *via* a specific TFRC-dependent iron uptake pathway.

To verify the functional specificity of SNX3 deletion in affecting the TFRC-dependent iron uptake pathway, we examined whether supplementation with ferric citrate (iron supplement) abrogated the ferroptosis protective effect in SNX3-silenced NRCMs. We found that ferric citrate supplements markedly decreased cell viability (Supporting Information Fig. S13A and S13B), significantly increased intracellular lipid peroxidation and Fe^{2+} levels (Fig. 8L, Fig. S13C), and seriously exacerbated mitochondrial dysfunction and damage (Fig. 8M, Fig. S13D).

In summary, these data demonstrated that SNX3 mediated ferroptosis by regulating the trafficking of TFRC in Dox-induced cardiomyopathy and that inhibition or induction of TFRC can ameliorate or exacerbate SNX3-induced ferroptosis, respectively.

4. Discussion

SNX3 has been identified by our laboratory as a promising therapeutic target in pathologic cardiac hypertrophy and is upregulated in the progression from cardiac hypertrophy to heart failure[34]. Interestingly, we showed that SNX3 expression was reduced in the Dox-induced cardiomyopathy mice model, indicating that the roles of SNX3 are varied in different types of heart diseases. This prompted us to investigate the effects of SNX3 on Dox-induced cardiomyopathy and the underlying mechanisms. *Snx3*-cKO mice showed attenuated Dox-induced cardiomyopathy, whereas *Snx3*-cTg mice presented myocardial injury and aggravated Dox-induced cardiomyopathy. Similar results were observed in cardiomyocytes infected with Ad-shSNX3 or Ad-SNX3 before Dox treatment, suggesting that SNX3 plays a deteriorative role in Dox-induced cardiomyopathy both *in vivo* and *in vitro*. It appears paradoxical that SNX3 expression is reduced in Dox-induced cardiomyopathy, while SNX3 loss attenuates Dox-induced cardiomyopathy. Since we found that SNX3 exacerbates the entry of a large number of iron ions into cells *via* interaction with TFRC while Dox transfers cytoplasmic iron ions into the mitochondria, thereby promoting ferroptosis. Thus, we speculated that a certain degree of SNX3 downregulation might be an insufficient compensatory mechanism against Dox-induced iron overload in the mitochondria. Another possible explanation is that SNX3 downregulation in Dox-treated cardiomyocytes may act as an important self-protection mechanism and a STOP signal, limiting the process of ferroptosis and myocardial injury.

Recent reports reveal that ferroptosis, but not other known forms of PCD (such as apoptosis and necroptosis) or regulated cell death (such as pyroptosis and parthanatos), is essential for Dox-induced cardiomyopathy[41−43]. Ferroptosis is morphologically, biochemically, and genetically different from other established forms of regulated cell death and is initiated by the iron-dependent accumulation of lipid peroxides[44]. Morphologically, the characteristics of ferroptosis are mitochondrial rupture and mitochondrial membrane potential reduction due to the imbalance of mitochondrial fission and fusion[45]. Biochemically, ferroptosis is caused by elevated levels of iron-dependent lipid peroxidation[46]. Consistent with previous reports, our observations confirm the importance of ferroptosis in Dox-induced cardiomyopathy, as indicated by the following results: (1) ferroptosis was induced in Dox-treated mice and cardiomyocytes; (2) two different small molecule ferroptosis inhibitors (iron chelator DFO and lipid radical scavenger Fer-1) blunted Dox-induced ferroptosis and myocardial injury; and (3) two distinct classical ferroptosis inducers (erastin and ferric citrate) significantly triggered ferroptosis and injury in cardiomyocytes. In addition, cardiac-specific SNX3 deficiency rescued Dox-induced ferroptosis, whereas cardiac-specific SNX3 overexpression was capable of exacerbating Dox-induced ferroptosis both *in vitro* and *in vivo*. This is not surprising because SNX3 and Dox induces ferroptosis in two distinct phases: SNX3 promotes the translocation of iron from extracellular to intracellular compartments, and Dox subsequently transfers intracellular iron into mitochondria. Thus, SNX3 and Dox may have a synergetic effect on the accumulation of iron in the mitochondria.

More importantly, we found that the aggravating effect of SNX3 on Dox-induced cardiomyopathy was mediated by ferroptosis induction. Iron overload has long been elucidated as a risk

MitoSox for MitoROS (scale bar: 20 μm). (K) Flow cytometry analysis of intracellular lipid peroxidation levels by C11-$BODIPY^{581/591}$ staining. (L, M) Typical pictures of Liperfluo staining (scale bar: 20 μm) and TEM (scale bar: 200 nm). Typical pictures of five independent experiments are shown. The data are shown as the mean ± SEM, $n = 3−5$ for the cell test. $^{*}P < 0.05$, $^{**}P < 0.01$, $^{***}P < 0.001$, $^{****}P < 0.0001$ *vs.* Vector group; $^{\#}P < 0.05$, $^{\#\#}P < 0.01$, $^{\#\#\#}P < 0.001$, $^{\#\#\#\#}P < 0.0001$ *vs.* vector + Dox group. See also Figs. S12 and S13.

factor for advanced cardiomyopathy[21,26,47], and the exploitation and verification of preclinical models of iron overload cardiomyopathy are significant for the discovery of new therapies for Dox-induced cardiomyopathy. Here, iron overload was discovered in a model of Dox-induced cardiomyopathy. Ferric citrate (iron supplement) supplements increased intracellular lipid peroxidation, Fe^{2+} levels, and ferroptosis. Additionally, the elevated iron levels in the Dox-treated group were reduced and exacerbated by SNX3 deficiency and SNX3 overexpression, respectively. The protective effect of SNX3 silence on Dox-induced cardiomyopathy was abrogated by ferroptosis inducers (erastin or ferric citrate), whereas SNX3-mediated cardiac injury was prevented by ferroptosis inhibitors (DFO or Fer-1). Our results suggest that SNX3 exacerbated Dox-induced ferroptosis and cardiomyopathy by mediating iron overload effects.

TFRC is a vital endogenous regulator of iron homeostasis[39,46]. The expression of TFRC is reduced in the hearts of cardiac-specific iron-regulatory protein 1/2 knockout mice, which increases susceptibility to myocardial infarction[16]. A lethal phenotype in cardiac-specific TFRC knockout mice was attributable to mitochondrial dysfunction caused by severe iron deficiency in the myocardium[32]. However, few studies have shown whether TFRC plays a part in Dox-induced ferroptosis and cardiomyopathy. In this study, TFRC knockdown inhibited iron absorption, thus preventing Dox-induced ferroptosis and cardiomyopathy, while TFRC overexpression mimicked the effects of Dox on the induction of ferroptosis and cardiomyopathy. TFRC overexpression abolished the protective effect of SNX3 knockdown on Dox-induced ferroptosis and cardiomyopathy. In contrast, TFRC deletion rescued SNX3-mediated ferroptosis and cardiac injury. The resistance to ferroptosis caused by SNX3 deficiency can be reversed by iron chelation supplementation. Furthermore, our results show that TFRC protein levels were upregulated *via* direct interaction with SNX3 in cardiomyocytes. Given that SNX3 regulates endocytic recycling of cargo proteins, we speculate that TFRC is sorted into recyclable endosomes by SNX3, accelerating the absorption of free iron, resulting in ferroptosis and finally deteriorating Dox-induced cardiomyopathy. Consistent with this notion, a previous study also showed that SNX3 regulates endocytic recycling of TFRC binds to an interface site between SNX3 and VPS26[27]. Of course, in addition to TFRC, there must be other target proteins of SNX3, which is also the focus of our future work.

SNX3 is the simplest subtype of the SNX family, consisting of an extremely conserved PX domain, mediates intracellular trafficking of cargo proteins (such as Wntless and CI-M6PR)[48]. It was previously believed that SNX3 mediates the retrograde transportation of cargo proteins from early endosomes to the TGN or PM through vesicle budding[33,48,49]. However, we recently reported that SNX3 also transports the cargo protein STAT3 into the nucleus in cardiomyocytes[34]. Here, we illustrate that TFRC may be a new cargo protein of SNX3, coregulating iron homeostasis and ferroptosis in Dox-induced cardiomyopathy. SNX3 may be involved in various heart diseases by transporting different cargo proteins, which is worthy of further exploration. We believe SNX3 has the potential for clinical translation, due to the important role of SNX3 both in Dox-induced cardiomyopathy in this study and in the progression from cardiac hypertrophy to heart failure previously identified by our laboratory.

In addition to intracellular iron level, ferroptosis is also regulated by several other key factors (including GPX4, FSP1, Hmox1, FTH, and DHODH) and is involved in heart disease[42,45,50]. Dox induces mitochondrial pathway-dependent ferroptosis by down-regulating GPX4, ultimately causing cardiomyopathy. Fth-deficient cardiomyocytes reduced the expression of SLC7A11 and resulted in severe heart damage[51]. Dexrazoxane prevented Dox-induced cardiotoxicity through HMGB1-regulated ferroptosis[52]. METTL14 exacerbated Dox-induced cardiomyocyte ferroptosis by regulating the KCNQ1OT1−miR-7-5p−TFRC axis[11]. Inhibition of Hmox1 decreased cardiac ferroptosis in sickle cell disease mice. Whether SNX3 is also linked to these signaling molecules in Dox-induced ferroptosis and cardiomyopathy merits further investigation. Although the significant reduction in SNX3 expression in Dox-induced cardiomyopathy seems to be contradictory to the increased expression of SNX3 in cardiac hypertrophy, SNX3 plays a deleterious role in both heart diseases. Considering that *Snx3*-cTg mice exhibited a certain degree of myocardial injury phenotype in the absence of pathological stimulation and further aggravated myocardial injury induced by Dox or ISO, we speculate that SNX3 might be sensitive to the severity of heart-related diseases, and the decrease in SNX3 expression might be an insufficient compensatory mechanism against strong Dox stimuli.

5. Conclusions

Collectively, our study reveals that the SNX3/TFRC axis plays a vital role in triggering iron-mediated ferroptosis and provides a potential new therapeutic strategy for Dox-induced cardiomyopathy by targeting SNX3.

Acknowledgments

We are grateful to Suowen Xu (Univ Sci & Technol China) for language editing of the article before submission. We thank Yuanfeng He (Sun Yat-sen University) for assistance with echocardiography. This work was supported by the National Natural Science Foundation of China (82173808, U21A20419, 82270500), Natural Science Foundation of Guangdong Province (2021B1515020100, China), Guangzhou Basic and Applied Basic Research Project (202206080007, China), Local Innovative and Research Teams Project of Guangdong Pearl River Talents Program (2017BT01Y093, China), Guangdong Provincial Key Laboratory of Construction Foundation (2017B030314030, China), and Academic promotion program of Shandong First Medical University (2019LJ003, China).

Author contributions

Peiqing Liu and Jing Lu designed and supervised research. Wenjing Yu, Yuehuai Hu, and Kaiteng Guo performed the experiments and acquired data. Xiaolei Zhang and Jiguo Zhang provided scientific advice and analysised of data. Dinghu Ma, Mingxia Peng, Yuemei Wang, Jing Zhang, and Panxia Wang performed several in animals experiments. Jing Lu and Wenjing Yu wrote the manuscript. Peiqing Liu critically amended modifications. All authors made essential recommendations and approved the final manuscript.

Conflicts of interest

The authors declare no conflict of interest.

Appendix A. Supporting information

Supporting data to this article can be found online at https://doi.org/10.1016/j.apsb.2023.08.016.

References

1. Vejpongsa P, Yeh ETH. Prevention of anthracycline-induced cardiotoxicity. *J Am Coll Cardiol* 2014;**64**:938−45.
2. Perez IE, Taveras Alam S, Hernandez GA, Sancassani R. Cancer therapy-related cardiac dysfunction: an overview for the clinician. *Clin Med Insights Cardiol* 2019;**13**:1179546819866445.
3. Li D, Yang Y, Wang S, He X, Liu M, Bai B, et al. Role of acetylation in doxorubicin-induced cardiotoxicity. *Redox Biol* 2021;**46**:102089.
4. Christidi E, Brunham LR. Regulated cell death pathways in doxorubicin-induced cardiotoxicity. *Cell Death Dis* 2021;**12**:339.
5. Zhang S, Liu X, Bawa-Khalfe T, Lu LS, Lyu YL, Liu LF, et al. Identification of the molecular basis of doxorubicin-induced cardiotoxicity. *Nat Med* 2012;**18**:1639−42.
6. Wallace KB, Sardao VA, Oliveira PJ. Mitochondrial determinants of doxorubicin-induced cardiomyopathy. *Circ Res* 2020;**126**:926−41.
7. Tadokoro T, Ikeda M, Ide T, Deguchi H, Ikeda S, Okabe K, et al. Mitochondria-dependent ferroptosis plays a pivotal role in doxorubicin cardiotoxicity. *JCI Insight* 2020;**5**:e132747.
8. Zhang T, Zhang Y, Cui M, Jin L, Wang Y, Lv F, et al. CaMKII is a RIP3 substrate mediating ischemia- and oxidative stress-induced myocardial necroptosis. *Nat Med* 2016;**22**:175−82.
9. Wang P, Wang L, Lu J, Hu Y, Wang Q, Li Z, et al. SESN2 protects against doxorubicin-induced cardiomyopathy *via* rescuing mitophagy and improving mitochondrial function. *J Mol Cell Cardiol* 2019;**133**:125−37.
10. Ji QX, Zeng FY, Zhou J, Wu WB, Wang XJ, Zhang Z, et al. Ferroptotic stress facilitates smooth muscle cell dedifferentiation in arterial remodelling by disrupting mitochondrial homeostasis. *Cell Death Differ* 2023;**30**:457−74.
11. Zhuang S, Ma Y, Zeng Y, Lu C, Yang F, Jiang N, et al. METTL14 promotes doxorubicin-induced cardiomyocyte ferroptosis by regulating the KCNQ1OT1−miR-7-5p−TFRC axis. *Cell Biol Toxicol* 2023;**35**:1015−35.
12. Dixon SJ, Lemberg KM, Lamprecht MR, Skouta R, Zaitsev EM, Gleason CE, et al. Ferroptosis: an iron-dependent form of non-apoptotic cell death. *Cell* 2012;**149**:1060−72.
13. Pinto NA, Abba MC, Laporte L, Pérez Sáez JM, Blidner AG, Torres NI, et al. Galectin-7 reprograms skin carcinogenesis by fostering innate immune evasive programs. *Cell Death Differ* 2023;**30**:906−21.
14. Lei G, Zhang YL, Koppula P, Liu XG, Zhang J, Lin SH, et al. The role of ferroptosis in ionizing radiation-induced cell death and tumor suppression. *Cell Res* 2020;**30**:146−62.
15. Ahola S, Rivera Mejías P, Hermans S, Chandragiri S, Giavalisco P, Nolte H, et al. OMA1-mediated integrated stress response protects against ferroptosis in mitochondrial cardiomyopathy. *Cell Metabol* 2022;**34**:1875.
16. Fang X, Ardehali H, Min J, Wang F. The molecular and metabolic landscape of iron and ferroptosis in cardiovascular disease. *Nat Rev Cardiol* 2023;**20**:7−23.
17. Liang C, Zhang XL, Yang MS, Dong XC. Recent progress in ferroptosis inducers for cancer therapy. *Adv Mater* 2019;**31**:e1904197.
18. Komai K, Kawasaki NK, Higa JK, Matsui T. The role of ferroptosis in adverse left ventricular remodeling following acute myocardial infarction. *Cells* 2022;**11**:1399.
19. Stockwell BR. Ferroptosis turns 10: emerging mechanisms, physiological functions, and therapeutic applications. *Cell* 2022;**185**:2401−21.
20. Rochette L, Dogon G, Rigal E, Zeller M, Cottin Y, Vergely C. Lipid peroxidation and iron metabolism: two corner stones in the homeostasis control of ferroptosis. *Int J Mol Sci* 2022;**24**:449.
21. Koleini N, Shapiro JS, Geier J, Ardehali H. Ironing out mechanisms of iron homeostasis and disorders of iron deficiency. *J Clin Invest* 2021;**131**:e148671.
22. Chen GQ, Benthani FA, Wu J, Liang DG, Bian ZX, Jiang XJ. Artemisinin compounds sensitize cancer cells to ferroptosis by regulating iron homeostasis. *Cell Death Differ* 2020;**27**:242−54.
23. Lakhal-Littleton S, Wolna M, Carr CA, Miller JJ, Christian HC, Ball V, et al. Cardiac ferroportin regulates cellular iron homeostasis and is important for cardiac function. *Proc Natl Acad Sci U S A* 2015;**112**:3164−9.
24. Gao M, Monian P, Quadri N, Ramasamy R, Jiang X. Glutaminolysis and transferrin regulate ferroptosis. *Mol Cell* 2015;**59**:298−308.
25. Ichikawa Y, Ghanefar M, Bayeva M, Wu R, Khechaduri A, Naga Prasad SV, et al. Cardiotoxicity of doxorubicin is mediated through mitochondrial iron accumulation. *J Clin Invest* 2014;**124**:617−30.
26. Hirota K. An intimate crosstalk between iron homeostasis and oxygen metabolism regulated by the hypoxia-inducible factors (HIFs). *Free Radic Biol Med* 2019;**133**:118−29.
27. Yang L, Tan W, Yang X, You Y, Wang J, Wen G, et al. Sorting nexins: a novel promising therapy target for cancerous/neoplastic diseases. *J Cell Physiol* 2021;**236**:3317−35.
28. Cullen PJ. Endosomal sorting and signalling: an emerging role for sorting nexins. *Nat Rev Mol Cell Biol* 2008;**9**:574−82.
29. van Weering JR, Sessions RB, Traer CJ, Kloer DP, Bhatia VK, Stamou D, et al. Molecular basis for SNX-BAR-mediated assembly of distinct endosomal sorting tubules. *EMBO J* 2012;**31**:4466−80.
30. Kovtun O, Leneva N, Bykov YS, Ariotti N, Teasdale RD, Schaffer M, et al. Structure of the membrane-assembled retromer coat determined by cryo-electron tomography. *Nature* 2018;**561**:561−4.
31. Harterink M, Port F, Lorenowicz MJ, McGough IJ, Silhankova M, Betist MC, et al. A SNX3-dependent retromer pathway mediates retrograde transport of the Wnt sorting receptor Wntless and is required for Wnt secretion. *Nat Cell Biol* 2011;**13**:914−23.
32. Cui Y, Carosi JM, Yang Z, Ariotti N, Kerr MC, Parton RG, et al. Retromer has a selective function in cargo sorting *via* endosome transport carriers. *J Cell Biol* 2019;**218**:615−31.
33. Zhang P, Wu Y, Belenkaya TY, Lin X. SNX3 controls Wingless/Wnt secretion through regulating retromer-dependent recycling of Wntless. *Cell Res* 2011;**21**:1677−90.
34. Lu J, Xu S, Huo Y, Sun D, Hu Y, Wang J, et al. Sorting nexin 3 induces heart failure *via* promoting retromer-dependent nuclear trafficking of STAT3. *Cell Death Differ* 2021;**28**:2871−87.
35. Wang P, Wang M, Hu Y, Chen J, Cao Y, Liu C, et al. Isorhapontigenin protects against doxorubicin-induced cardiotoxicity *via* increasing YAP1 expression. *Acta Pharm Sin B* 2021;**11**:680−93.
36. Fang X, Wang H, Han D, Xie E, Yang X, Wei J, et al. Ferroptosis as a target for protection against cardiomyopathy. *Proc Natl Acad Sci U S A* 2019;**116**:2672−80.
37. Carvalho FS, Burgeiro A, Garcia R, Moreno AJ, Carvalho RA, Oliveira PJ. Doxorubicin-induced cardiotoxicity: from bioenergetic failure and cell death to cardiomyopathy. *Med Res Rev* 2014;**34**:106−35.
38. Yang Y, Luo M, Zhang K, Zhang J, Gao T, Connell DO, et al. Nedd4 ubiquitylates VDAC2/3 to suppress erastin-induced ferroptosis in melanoma. *Nat Commun* 2020;**11**:433.
39. Fisher AL, Wang CY, Xu Y, Joachim K, Xiao X, Phillips S, et al. Functional role of endothelial transferrin receptor 1 in iron sensing and homeostasis. *Am J Hematol* 2022;**97**:1548−59.
40. Cronin SJF, Woolf CJ, Weiss G, Penninger JM. The role of iron regulation in immunometabolism and immune-related disease. *Front Mol Biosci* 2019;**6**:116.
41. Wang X, Chen X, Zhou W, Men H, Bao T, Sun Y, et al. Ferroptosis is essential for diabetic cardiomyopathy and is prevented by sulforaphane *via* AMPK/NRF2 pathways. *Acta Pharm Sin B* 2022;**12**:708−22.
42. Kong N, Chen X, Feng J, Duan T, Liu S, Sun X, et al. Baicalin induces ferroptosis in bladder cancer cells by downregulating FTH1. *Acta Pharm Sin B* 2021;**11**:4045−54.
43. He H, Wang L, Qiao Y, Yang B, Yin D, He M. Epigallocatechin-3-gallate pretreatment alleviates doxorubicin-induced ferroptosis and cardiotoxicity by upregulating AMPK alpha 2 and activating adaptive autophagy. *Redox Biol* 2021;**48**:102185.

44. Stockwell BR, Friedmann Angeli JP, Bayir H, Bush AI, Conrad M, Dixon SJ, et al. Ferroptosis: a regulated cell death nexus linking metabolism, redox biology, and disease. *Cell* 2017; **171**:273−85.
45. Ta N, Qu C, Wu H, Zhang D, Sun T, Li Y, et al. Mitochondrial outer membrane protein FUNDC2 promotes ferroptosis and contributes to doxorubicin-induced cardiomyopathy. *Proc Natl Acad Sci U S A* 2022; **119**:e2117396119.
46. Tang D, Chen X, Kang R, Kroemer G. Ferroptosis: molecular mechanisms and health implications. *Cell Res* 2021;**31**:107−25.
47. Menon AV, Liu J, Tsai HP, Zeng L, Yang S, Asnani A, et al. Excess heme upregulates heme oxygenase 1 and promotes cardiac ferroptosis in mice with sickle cell disease. *Blood* 2022;**139**:936−41.
48. Li J, Li C, Zhang D, Shi D, Qi M, Feng J, et al. SNX13 reduction mediates heart failure through degradative sorting of apoptosis repressor with caspase recruitment domain. *Nat Commun* 2014;**5**:5177.
49. Johannes L, Wunder C. The SNXy flavours of endosomal sorting. *Nat Cell Biol* 2011;**13**:884−6.
50. Jiang X, Stockwell BR, Conrad M. Ferroptosis: mechanisms, biology and role in disease. *Nat Rev Mol Cell Biol* 2021;**22**:266−82.
51. Fang X, Cai Z, Wang H, Han D, Cheng Q, Zhang P, et al. Loss of cardiac Ferritin H facilitates cardiomyopathy *via* Slc7a11-mediated ferroptosis. *Circ Res* 2020;**127**:486−501.
52. Zhang H, Wang Z, Liu Z, Du K, Lu X. Protective effects of dexazoxane on rat ferroptosis in doxorubicin-induced cardiomyopathy through regulating HMGB1. *Front Cardiovasc Med* 2021;**8**:685434.